Broadband MIMO-OFDM Wireless Communications

GORDON L. STÜBER, FELLOW, IEEE, JOHN R. BARRY, MEMBER, IEEE,
STEVE W. MCLAUGHLIN, SENIOR MEMBER, IEEE, YE (GEOFFREY) LI, SENIOR MEMBER, IEEE,
MARY ANN INGRAM, SENIOR MEMBER, IEEE, AND THOMAS G. PRATT, MEMBER, IEEE

Invited Paper

Orthogonal frequency division multiplexing (OFDM) is a popular method for high data rate wireless transmission. OFDM may be combined with antenna arrays at the transmitter and receiver to increase the diversity gain and/or to enhance the system capacity on time-variant and frequency-selective channels, resulting in a multiple-input multiple-output (MIMO) configuration. This paper explores various physical layer research challenges in MIMO-OFDM system design, including physical channel measurements and modeling, analog beam forming techniques using adaptive antenna arrays, space–time techniques for MIMO-OFDM, error control coding techniques, OFDM preamble and packet design, and signal processing algorithms used for performing time and frequency synchronization, channel estimation, and channel tracking in MIMO-OFDM systems. Finally, the paper considers a software radio implementation of MIMO-OFDM.

Keywords—Adaptive antennas, broadband wireless, multiple-input multiple-output (MIMO), orthogonal frequency division multiplexing (OFDM), software radio, space–time coding, synchronization.

I. INTRODUCTION

Orthogonal frequency division multiplexing (OFDM) has become a popular technique for transmission of signals over wireless channels. OFDM has been adopted in several wireless standards such as digital audio broadcasting (DAB), digital video broadcasting (DVB-T), the IEEE 802.11a [1] local area network (LAN) standard and the IEEE 802.16a [2] metropolitan area network (MAN) standard. OFDM is also being pursued for dedicated short-range communications (DSRC) for road side to vehicle communications and as a potential candidate for fourth-generation (4G) mobile wireless systems.

OFDM converts a frequency-selective channel into a parallel collection of frequency flat subchannels. The subcarriers have the minimum frequency separation required to maintain orthogonality of their corresponding time domain waveforms, yet the signal spectra corresponding to the different subcarriers overlap in frequency. Hence, the available bandwidth is used very efficiently. If knowledge of the channel is available at the transmitter, then the OFDM transmitter can adapt its signaling strategy to match the channel. Due to the fact that OFDM uses a large collection of narrowly spaced subchannels, these adaptive strategies can approach the ideal water pouring capacity of a frequency-selective channel. In practice this is achieved by using adaptive bit loading techniques, where different sized signal constellations are transmitted on the subcarriers.

OFDM is a block modulation scheme where a block of N information symbols is transmitted in parallel on N subcarriers. The time duration of an OFDM symbol is N times larger than that of a single-carrier system. An OFDM modulator can be implemented as an inverse discrete Fourier transform (IDFT) on a block of N information symbols followed by an analog-to-digital converter (ADC). To mitigate the effects of intersymbol interference (ISI) caused by channel time spread, each block of N IDFT coefficients is typically preceded by a cyclic prefix (CP) or a guard interval consisting of G samples, such that the length of the CP is at least equal to the channel length. Under this condition, a linear convolution of the transmitted sequence and the channel is converted to a circular convolution. As a result, the effects of the ISI are easily and completely eliminated. Moreover, the approach enables the receiver to use fast signal processing transforms such as a fast Fourier transform (FFT) for OFDM implementation [3]. Similar techniques can be employed in single-carrier systems as well, by preceding each transmitted data block of length N by a CP of length G, while using frequency-domain equalization at the receiver.
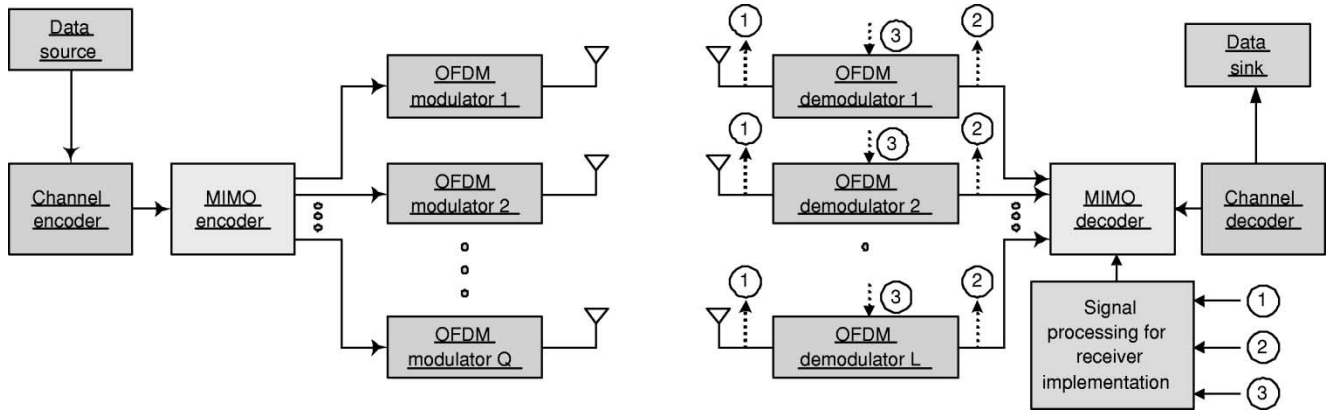
Fig. 1. $Q \times L$ MIMO-OFDM system, where Q and L are the numbers of inputs and outputs, respectively.

Multiple antennas can be used at the transmitter and receiver, an arrangement called a multiple-input multiple-output (MIMO) system. A MIMO system takes advantage of the spatial diversity that is obtained by spatially separated antennas in a dense multipath scattering environment. MIMO systems may be implemented in a number of different ways to obtain either a diversity gain to combat signal fading or to obtain a capacity gain. Generally, there are three categories of MIMO techniques. The first aims to improve the power efficiency by maximizing spatial diversity. Such techniques include delay diversity, space–time block codes (STBC) [4], [5] and space–time trellis codes (STTC) [6]. The second class uses a layered approach to increase capacity. One popular example of such a system is V-BLAST suggested by Foschini *et al.* [7] where full spatial diversity is usually not achieved. Finally, the third type exploits the knowledge of channel at the transmitter. It decomposes the channel coefficient matrix using singular value decomposition (SVD) and uses these decomposed unitary matrices as pre- and post-filters at the transmitter and the receiver to achieve near capacity [8].

OFDM has been adopted in the IEEE802.11a LAN and IEEE802.16a LAN/MAN standards. OFDM is also being considered in IEEE802.20a, a standard in the making for maintaining high-bandwidth connections to users moving at speeds up to 60 mph. The IEEE802.11a LAN standard operates at raw data rates up to 54 Mb/s (channel conditions permitting) with a 20-MHz channel spacing, thus yielding a bandwidth efficiency of 2.7 b/s/Hz. The actual throughput is highly dependent on the medium access control (MAC) protocol. Likewise, IEEE802.16a operates in many modes depending on channel conditions with a data rate ranging from 4.20 to 22.91 Mb/s in a typical bandwidth of 6 MHz, translating into a bandwidth efficiency of 0.7 to 3.82 bits/s/Hz. Recent developments in MIMO techniques promise a significant boost in performance for OFDM systems. Broadband MIMO-OFDM systems with bandwidth efficiencies on the order of 10 b/s/Hz are feasible for LAN/MAN environments. The physical (PHY) layer techniques described in this paper are intended to approach 10 b/s/Hz bandwidth efficiency.

This paper discuss several PHY layer aspects broadband MIMO-OFDM systems. Section II describes the basic MIMO-OFDM system model. All MIMO-OFDM receivers must perform time synchronization, frequency offset estimation, and correction and parameter estimation. This is generally carried out using a preamble consisting of one or more training sequences. Once the acquisition phase is over, receiver goes into the tracking mode. Section III provides an overview of the signal acquisition process and investigates sampling frequency offset estimation and correction in Section IV. The issue of channel estimation is treated in Section V. Section VI considers space–time coding techniques for MIMO-OFDM, while Section VII discusses coding approaches. Adaptive analog beam forming approaches can be used to provide the best possible MIMO link. Section VIII discusses various strategies for beamforming. Section IX very briefly considers medium access control issues. Section X discusses a software radio implementation for MIMO-OFDM. Finally, Section XI wraps up with some open issues concluding remarks.

II. MIMO-OFDM SYSTEM MODEL

A multicarrier system can be efficiently implemented in discrete time using an inverse FFT (IFFT) to act as a modulator and an FFT to act as a demodulator. The transmitted data are the "frequency" domain coefficients and the samples at the output of the IFFT stage are "time" domain samples of the transmitted waveform. Fig. 1 shows a typical MIMO-OFDM implementation.

Let $\mathbf{X} = \{X_0, X_1, \ldots, X_{N-1}\}$ denote the length-N data symbol block. The IDFT of the date block $\mathbf{X}$ yields the time domain sequence $\mathbf{x} = \{x_0, x_1, \ldots, x_{N-1}\}$, i.e.,

$$x_n = \text{IFFT}_N\{X_k\}(n). \tag{1}$$

To mitigate the effects of channel delay spread, a guard interval comprised of either a CP or suffix is appended to the sequence $\mathbf{X}$. In case of a CP, the transmitted sequence with guard interval is

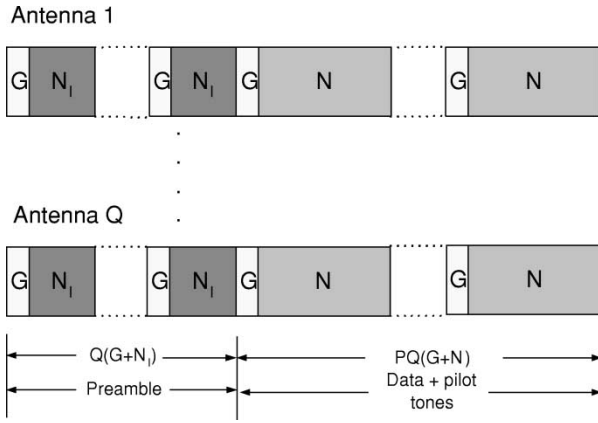$$x_n^g = x_{(n)_N}, \; n = -G, \ldots, -1, 0, 1, \ldots, N-1 \tag{2}$$

Fig. 2. Frame structure for the $Q \times L$ OFDM system.

where G is the guard interval length in samples, and $(n)_N$ is the residue of n modulo N. The OFDM complex envelope is obtained by passing the sequence $\mathbf{x}^g$ through a pair of ADCs (to generate the real and imaginary components) with sample rate $1/T$ s, and the analog I and Q signals are upconverted to an RF carrier frequency. To avoid ISI, the CP length G must equal or exceed the length of the discrete-time channel impulse response M. The time required to transmit one OFDM symbol $T_s = NT + GT$ is called the OFDM symbol time. The OFDM signal is transmitted over the passband RF channel, received, and downconverted to base band. Due to the CP, the discrete linear convolution of the transmitted sequence with the channel impulse response becomes a circular convolution. Hence, at the receiver the initial G samples from each received block are removed, followed by an N-point discrete Fourier transform (DFT) on the resulting sequence.

The frame structure of a typical MIMO-OFDM system is shown in Fig. 2. The OFDM preamble consists of Q training symbols of length $N_I + G$, where $G \leq N_I \leq N$, $N_I = N/I$ and I an integer that divides N. Often the length of the guard interval in the training period is doubled; for example, in IEEE802.16a [1], to aid in synchronization, frequency offset estimation and equalization for channel shortening in cases where the length of the channel exceeds the length of the guard interval.

First consider the preamble portion of the OFDM frame. The length-$N_I + G$ preamble sequences are obtained by exciting every Ith coefficient of a length-N frequency-domain vector with a nonzero training symbol from a chosen alphabet (the remainder are set to zero). The frequency-domain training sequences transmitted from the ith antenna are $\{S_k^{(q)}\}_{k=1}^N$, where $q = (c-1)Q + i$ and $c = 1, 2, \ldots, Q$. The individual length-N_I time domain training sequences are obtained by taking an N-point IDFT of the sequence $\{S_k^{(q)}\}_{k=1}^N$, keeping the first N_I time-domain coefficients and discarding the rest. A CP is appended to each length-N_I time-domain sequence. Let $\mathbf{H}_{ij}$ be the vector of subchannel coefficients between the ith transmit and the jth receive antenna and let $\{R_k^{(l)}\}_{k=0}^{N_I-1}$ be the received sample sequence at the lth receiver antenna. After removing the guard interval,

the received samples $\{R_k^{(l)}\}_{k=0}^{N_I-1}$ are repeated I times and demodulated using an N-point FFT as

$$R_k^{(l)} = \text{FFT}_N\{r^{(l)}\}(k) \tag{3}$$

$$= \sum_{q=1}^{Q} H_k^{(q,l)} S_k^{(q)} + W_k^{(l)} \tag{4}$$

where $k = 0, \ldots, N-1$. The demodulated OFDM sample matrix $\mathbf{R}_k$ of dimension $(Q \times L)$ for the kth subcarrier can be expressed in terms of the transmitted sample matrix $\mathbf{S}_k$ of dimension $(Q \times Q)$, the channel coefficient matrix $\mathbf{H}_k$ of dimension $(Q \times L)$ and the additive white Gaussian noise matrix $\mathbf{W}_k$ of dimension $(Q \times L)$ [24] as

$$\mathbf{R}_{k,Q \times L} = \mathbf{S}_{k,Q \times Q} \cdot \mathbf{H}_{k,Q \times L} + \mathbf{W}_{k,Q \times L} \tag{5}$$

where $\mathbf{R}$, $\mathbf{H}$, and $\mathbf{W}$ can viewed as either a collection of N matrices of dimension $Q \times L$ or as a collection of $Q \times L$ vectors of length N.

A. Preamble Design for MIMO-OFDM Systems

Least square channel estimation schemes require that all $Q \times N_I$ training symbol matrices $\mathbf{S}^{(q)}$, $q = (c-1)Q + k$, $k = 1, \ldots, N_I$ be unitary so that only Q OFDM symbols are needed for channel estimation [25]. A straightforward solution is to make each $\mathbf{S}_k$ a diagonal matrix. However, the power of the preamble needs to be boosted by $10 \log_{10} Q$ dB in order to achieve a performance similar to the case when the preamble signal is transmitted from all the antennas. This has the undesirable effect of increasing the dynamic range requirements of the power amplifiers. Hence, methods are required so that sequences can be transmitted from all the antennas while still having unitary $\mathbf{S}_k$ matrices. One approach adapts the work by Tarokh *et al.* on space–time block codes [5], [26]. For $Q = 2$, 4, and 8, orthogonal designs exist. For example, for $Q = 2$ and 4, we can choose the preamble structures of the form

$$\mathbf{S}_{AS} = \begin{bmatrix} \mathbf{S}_1 & \mathbf{S}_1 \\ -\mathbf{S}_1 & \mathbf{S}_1 \end{bmatrix} \tag{6}$$

$$\mathbf{S}_{TS} = \begin{bmatrix} \mathbf{S}_1 & \mathbf{S}_1 & \mathbf{S}_1 & \mathbf{S}_1 \\ -\mathbf{S}_1 & \mathbf{S}_1 & -\mathbf{S}_1 & \mathbf{S}_1 \\ -\mathbf{S}_1 & \mathbf{S}_1 & \mathbf{S}_1 & -\mathbf{S}_1 \\ -\mathbf{S}_1 & -\mathbf{S}_1 & \mathbf{S}_1 & \mathbf{S}_1 \end{bmatrix} \tag{7}$$

where $\mathbf{S_1}$ is the length-N_I vector S_k, $k = 1 \ldots N_I$. This results in unitary $\mathbf{S}_k$ matrices. As it turns out, transmitting the same sequence from all the antennas in this fashion is advantageous when performing synchronization. A similar structure for $Q = 8$ exists. For other values of Q, a least squares (LS) solution for the channel estimates can be obtained by either transmitting more than Q training sequences or by making the training symbol matrices unitary by using a Gram–Schmidt orthonormalization procedure as described in [24].

B. Pilot Insertion

Channel coefficients require constant tracking. This is aided by inserting known pilot symbols at fixed or variable subcarrier positions. For example, the IEEE 802.16a
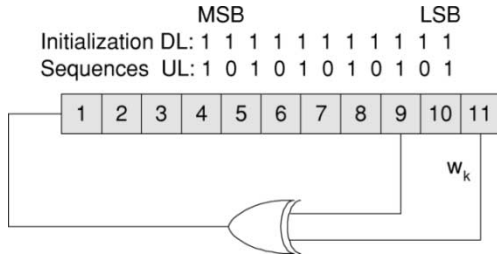
Fig. 3. Pilot tone generation.

standard recommends the insertion of eight pilot tones at fixed positions on subcarriers [12, 36, 60, 84, 172, 196, 220, 244] (assuming $N = 256$). Fig. 3 shows the method for generating the pilot sequences used in the IEEE 802.16a standard. In the downlink (DL) and the uplink (UL), the shift register is initialized with sequences as shown. A 0 at the output P_n is mapped to $+1$ and a 1 is mapped to -1. For a MIMO system with $Q = 2$ and 4 antennas, the pilot sequences p_n can be coded over space and time to form structures in (6) and (7), respectively, thereby admitting a simple LS channel estimate. For more information on the pilot sequence construction, readers can refer to [27].

III. SYNCHRONIZATION IN THE ACQUISITION MODE

Time and frequency synchronization can be performed sequentially in the following steps [28].

Step 1) *Coarse Time Synchronization and Signal Detection*—Coarse time acquisition and signal detection locates the start of an OFDM frame over an approximate range of sample values. Due to the presence of the CP (or suffix), coarse time acquisition during the preamble can be performed by correlating the received samples that are at a distance of N_I from each other over a length-G window ([25], [29]), viz.

$$n_{j,\text{coarse}} = \arg \underbrace{\max}_{n} \{\phi_{j,n}\}. \tag{8}$$

where $\phi_{j,n} = \sum_{k=0}^{G-1} (r_{j,n+k}^* \cdot r_{j,n+k+N_I})$. In addition to maximizing $\phi_{j,n}$, it should also exceed a certain threshold to reduce the probability of false alarm (P_{FA}). We chose the threshold to be 10% of the incoming signal energy of the correlation window.

Step 2) *Frequency Offset Estimation in the Time Domain*—Any frequency offset between the transmitter and the receiver local oscillators is reflected in the time domain sequence as a progressive phase shift $\theta = 2\pi\gamma N_I/N$, where γ is the frequency offset and is defined as the ratio of the actual frequency offset to the intercarrier spacing. A frequency offset estimate of up to $\pm I/2$ subcarrier spacings can be obtained based on the phase of the autocorrelation function in (8) as follows:

$$\hat{\gamma}_j = \frac{I}{2\pi} \angle \{\phi_{n_{j,\text{coarse}}}\} \tag{9}$$

where $n_{j,\text{coarse}}$ is the optimum coarse timing acquisition instant and $I = N/N_I$. The frequency offset can then be removed from the received sample sequence by multiplying it with $\exp\{-j2\pi\hat{\gamma}n/N_I\}$ during the preamble and $\exp\{-j2\pi\hat{\gamma}n/N\}$ during the data portion. Note that by reducing the length of the training symbol by a factor of I, the range of the frequency offset estimate in the time domain can be increased by a factor of I.

Step 3) *Residual Frequency Offset Correction*—Should the range of the time domain frequency offset estimation be insufficient, frequency-domain processing can be used. Suppose that the same frequency-domain training sequence $\{S_k^{(q)}\}_{k=1}^N$ is transmitted from all the antennas. The residual frequency offset, that is, an integer multiple of the subcarrier spacing, can be estimated by computing a cyclic cross-correlation of $\{S_k^{(q)}\}_{k=1}^N$ with the received, frequency corrected (from Step II), demodulated symbol sequence, viz.,

$$\chi_k = \sum_{n=0}^{N-1} S^{(q)*}_{(k+n)_N} R^{(1)c}_n \quad k=0,1,\ldots,N-1 \tag{10}$$

where

$$R^{(1)c}_n = \text{FFT}_N \left\{ r_n^{(1)} e^{j2\pi\hat{\gamma}_{\text{ML}}n/N_I} \right\}. \tag{11}$$

The residual frequency offset is estimated as $\hat{\Gamma} = \arg\max\{|\chi_k|\}$, $k = 0, 1, \ldots, N - 1$. Note that the fractional part of the relative frequency offset is estimated in the time domain in Step II while the integer part is estimated in the frequency domain in Step III.

Step 4) *Fine Time Synchronization*—Fine time acquisition locates the start of the useful portion of the OFDM frame to within a few samples. Once the frequency offset is removed, fine time synchronization can be performed by cross correlating the frequency corrected samples with the transmitted preamble sequences. The fine time synchronization metric is

$$n_{j,\text{fine}} = \arg \underbrace{\max}_{n} \{\psi_{j,n}\} \tag{12}$$

where $\psi_{j,n} = \sum_{q=1}^{Q} \left| \sum_{k=0}^{N_I-1} (s_{q,k}^* \cdot r_{j,n+k}) \right|$. For systems using two and four and eight transmit antennas using the orthogonal designs discussed in Section II-A, only one cross correlator is needed per receiver antenna. Once again the threshold is set at 10% of the energy contained in N_I received samples. Since fine time synchronization is computationally expensive process, it is carried out for a small window centered around the coarse time synch. instant $n_{j,\text{coarse}}$.

Finally, the net time synchronization instant for the entire receiver is selected to be $n_{\text{opt}} = (1/L) \sum_{j=1}^{L} n_{j,\text{fine}}$. An added negative offset of a few samples is applied to the

Table 1
SUI-4 Channel Model

	Tap 1	Tap 2	Tap 3	Units
Delay	0	1.5	4.0	μs
Power (omni ant.)	0	-4	-8	dB
Doppler f_m	0.2	0.15	0.25	Hz

fine time synchronization instant in order to ensure that the OFDM windows for all the receivers falls into an ISI-free zone.

A. Example

Consider a 2×2 and a 4×4 broadband MIMO-OFDM system [2] operating at a carrier frequency of 5.8 GHz on the SUI-4 channel shown in Table 1. The OFDM signal occupies a bandwidth of 4.0 MHz. The uncorrected frequency offset $(\Gamma + \gamma)$ is 1.25 subcarrier spacings. The OFDM blocksize is $N = 256$, and the guard interval is kept at $N/4 = 64$. Out of 256 tones, the dc tone and 55 other tones at the band edges are set to zero. Hence, the number of used tones $N_u = 200$. The length of the sequences used in the preamble is varied from N to $N/2$ to $N/4$. The preamble insertion period P is chosen to be ten. STBCs are used to encode the data. For a 2×2 system, the Alamouti STBC is used with code rate 1, whereas for a 4×4 system, code rate is 3/4 [26]. In the data mode, each of the tones is modulated using a 16-QAM constellation and no channel coding is employed. LS channel estimates obtained using the preamble are used to process the entire frame [28]. For training sequences of length $N_I < N$, frequency-domain linear interpolation and extrapolation are used. Afterwards, frequency-domain smoothing is used, such that channel estimates at the band-edges are kept as they are, whereas all the other channel estimates are averaged using

$$\hat{H}_k^{(q,j)} = \frac{\bar{H}_{k-1}^{(q,j)} + \bar{H}_{k+1}^{(q,j)}}{2}. \quad (13)$$

Fig. 4 shows the coarse and fine time synchronization performance for a 4×4 MIMO-OFDM system with $N_I = 128$, $I = 2$, and signal-to-noise ratio (SNR) of 10 dB.

Fig. 5 shows the overall bit error rate (BER) performance of a 2×2 MIMO-OFDM system using the suggested algorithms.

IV. SAMPLE FREQUENCY OFFSET CORRECTION AND TRACKING

MIMO-OFDM schemes that use coherent detection need accurate channel estimates. Consequently, the channel coefficients must be tracked in a system with high Doppler. In the broadband fixed wireless access (BFWA) system IEEE

802.16a, the channel is nearly static. However, channel variations are still expected due to the presence of sampling frequency offset between transmitter and the receiver RF oscillators. Generally, the components in the customer premises equipment (CPE) have a low tolerance with typical drift of 20 parts per million (ppm). This means a signal with a BW of 4 MHz produces an offset of 80 samples for every 1 s of transmission. Sample frequency offset causes phase rotation, amplitude distortion and loss in synchronization.

Even after successful signal acquisition and synchronization, the OFDM system must guard against sample frequency offset (SFO) and phase offset. It must also guard against drift in the RF local oscillator and sampling clock frequency with time [30].

Let $T' \neq T$ be the sampling time at the receiver and let $\beta = (T' - T)/T$ be the normalized offset in the sampling time. The received and demodulated OFDM symbol with the sampling time offset can be approximated by (14), at the bottom of the page. where $k = 0, \ldots, N-1, l = (j-1)Q+g$ and $g = 1, 2, \ldots, Q$ is the running index of the OFDM symbol in time, and $\text{sinc}(x) = \sin(\pi x)/\pi x$.

Due to the sampling frequency offset β, the received demodulated symbol suffers phase rotation as well as amplitude distortion. In general, the value of β is very small. For example, for a sampling clock tolerance of 20 ppm and sampling frequency $f_s = 8$ MHz, $\beta = 2 \times 10^{-5}$. Hence, $\text{sinc}(k\beta) \approx 1$ and its effect is negligible. With this assumption, the demodulated OFDM sample matrix $\mathbf{R}_k$ in (5) becomes

$$\mathbf{R}_{k,Q \times L} = \mathbf{\Lambda}_{k,Q \times Q} \cdot \mathbf{S}_{k,Q \times Q} \cdot \mathbf{H}_{k,Q \times L} + \mathbf{W}_{k,Q \times L}. \quad (15)$$

where $\mathbf{\Lambda}_{k,Q \times Q}$ is diagonal matrix representing the phase rotations of the received demodulated samples due to the presence of sampling frequency offset.

A. Sample Frequency Offset Estimation

If the MIMO-OFDM transmission is being carried out in blocks of Q OFDM symbols, then phase rotation between consecutive blocks of OFDM symbols increases in a linear fashion. Hence let the received sample matrix corresponding to the preamble be given by

$$\mathbf{R}_k^{\text{preamble}} = \mathbf{\Lambda}_k^{\text{preamble}} \cdot \mathbf{S}_k^{\text{preamble}} \cdot \mathbf{H}_k + \mathbf{W}_k. \quad (16)$$

The received sample matrix for the next block of Q OFDM symbols corresponding to the pilot tones is then given by

$$\mathbf{R}_k^p = \exp\left\{\frac{j2\pi Qk\beta(N+G)}{N}\right\} \times \mathbf{\Lambda}_k^{\text{preamble}} \cdot \mathbf{S}_k^p \cdot \mathbf{H}_k + \mathbf{W}_k. \quad (17)$$

If the channel does not change much for $2Q$ consecutive blocks of OFDM symbols as is the case for wireless

$$R_{g,k}^{(l)} = \sum_{q=1}^{Q} \exp\left\{\frac{j2\pi\beta gk(N+G)}{N}\right\} \text{sinc}(\beta k) \times H_{q,k}^{(l)} S_k^{(q)} + W_{k,\text{AWGN}}^{(l)} + W_{k,\text{ICI}} \quad (14)$$
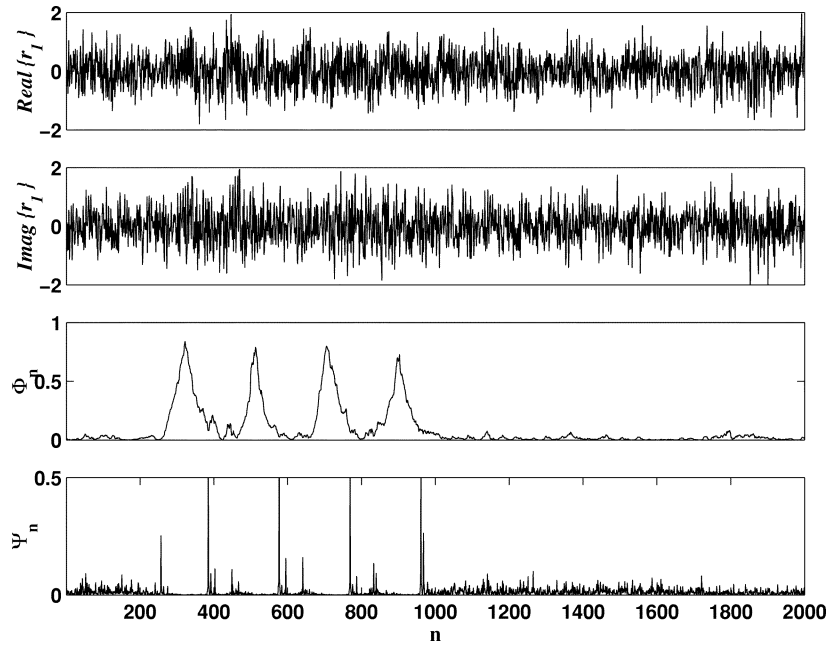
Fig. 4. Coarse and fine time synchronization for a 4×4 system with $N_I = 128$, SNR $= 10$ dB, freq. off. $\Gamma + \gamma = 1 + 0.25$. Steps IB, IIIB.
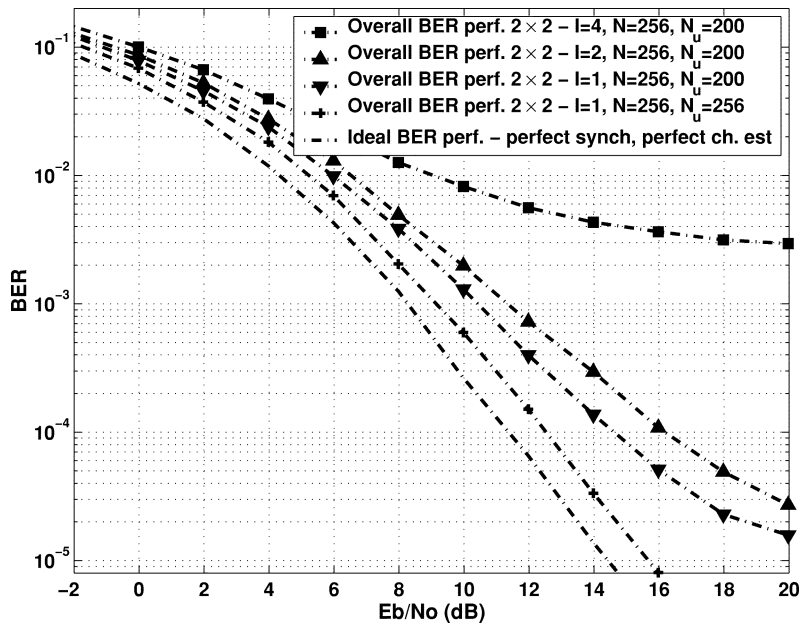

Fig. 5. Uncoded BER as a function of SNR for a 2×2 system using 16-QAM modulation, $P = 10$.

LAN/MAN applications, then we can correlate $\mathbf{R}_k^{\text{preamble}}$ and $\mathbf{R}_k^p$ to obtain an initial estimate of β per subcarrier as

$$\hat{\beta}_k^{\text{initial}} = \frac{\angle \text{trace}[\mathbf{R}_k^{H \text{ preamble}} \mathbf{R}_k^p]}{\frac{2\pi Q k(N+G)}{N}}$$

$$= \frac{\angle \sum_{l=1}^{L} |R_{l,l}|^2 \exp\left\{\frac{j2\pi\beta Q k(N+G)}{N}\right\}}{\frac{2\pi Q k(N+G)}{N}}. \quad (18)$$

This estimate of the sampling frequency offset estimate is then averaged over all the subcarriers.

B. Channel Estimation

Once initial estimates of β are obtained, channel estimation can be carried out using the LS technique as

$$\hat{\mathbf{H}}_k = \mathbf{B}_k^H (\mathbf{B}_k \mathbf{B}_k^H)^{-1} \mathbf{R}_k, \quad (19)$$

where $\mathbf{B}_k = \mathbf{\Lambda}_k \mathbf{S}_k$. This ensures that the initial effect of the sampling frequency offset is taken into account when the channel is estimated. More elaborate channel estimation schemes are considered in Section V.
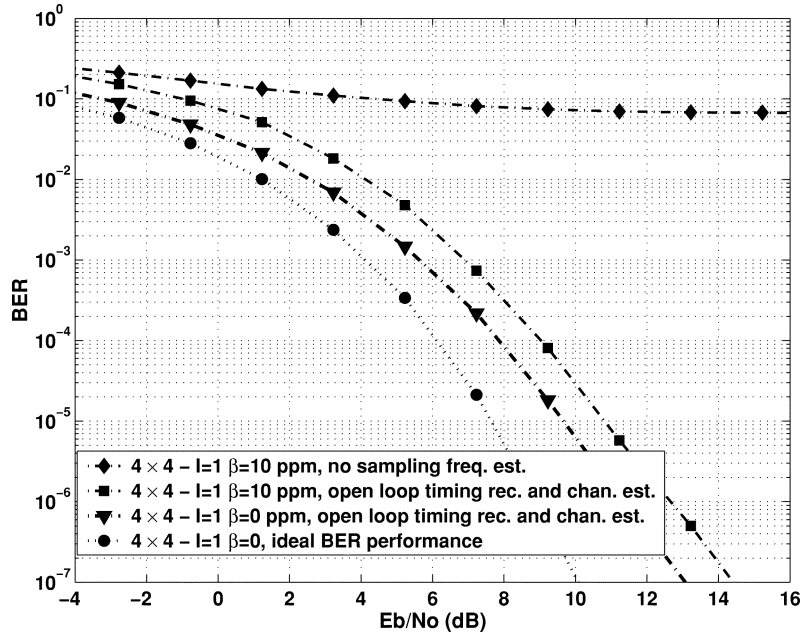
Fig. 6. BER performance for a 4×4 system with $\beta = 0$ and 10 ppm, with frame length of 80 OFDM symbols.

C. Sampling Frequency Offset Tracking

Once initial estimates of β are obtained, open loop sampling frequency offset estimation is obtained by minimizing the metric

$$\min \left(\text{trace} \left[(\mathbf{R}_k - \mathbf{\Lambda}_k \mathbf{C}_k^p)^H (\mathbf{R}_k - \mathbf{\Lambda}_k \mathbf{C}_k^p) \right] \right) \qquad (20)$$

where $\mathbf{C}_k^p = \mathbf{S}_k^p \mathbf{H}_k$. This results in the LS solution of the type

$$\hat{\mathbf{\Lambda}}_k = \mathbf{R}_k \mathbf{C}_k^{p\,H} (\mathbf{C}_k^p \mathbf{C}_k^{p\,H} + \delta \mathbf{I})^{-1} \qquad (21)$$

where δ is a small number of the order of 1×10^{-5} introduced to guard against ill-conditioned matrices and $\mathbf{I}$ is the identity matrix. If the variance of the noise at the receiver is known then this factor can be applied instead of δ. From $\hat{\mathbf{\Lambda}}_k$, the new value of sampling frequency offset may be extracted by correlating the diagonal elements of the $\hat{\mathbf{\Lambda}}_k$ matrix as

$$\hat{\beta}_k^{\text{new}} = \frac{\angle \left\{ \sum_{q=1}^{Q-1} \hat{\mathbf{\Lambda}}_{q,q,k}^* \hat{\mathbf{\Lambda}}_{q+1,q+1,k} \right\}}{\frac{2\pi k (N+G)}{N}}. \qquad (22)$$

The new value of $\hat{\beta}_k^{\text{new}}$ is then passed through a first-order low-pass filter and the output of the filter is used to obtain the filtered estimate of β. This then is used to form the new estimate $\hat{\mathbf{\Lambda}}_k^{\text{new}}$. The sampling frequency offset in the tracking mode is then compensated for as $\hat{\mathbf{R}}_k^{\text{new}} = (\hat{\mathbf{\Lambda}}_k^{\text{new}})^{-1} \mathbf{R}_k$.

D. Example

Simulations are carried out for the same 4×4 broadband fixed wireless access system described in Section III. The sampling frequency offset β is 10 parts per million (ppm) and is allowed to vary around that value in a random walk. Hence $\beta = 10$ ppm $+ \mathcal{N}(0, 1/10^6$ ppm). Fig. 6 shows the

BER results. The bottom curve is the ideal results with perfect synchronization and channel estimation and zero sampling frequency offset. The next curve up shows the performance with synchronization and channel estimation, but without any sampling frequency offset present in the system. The next curve up shows the performance with synchronization, channel estimation, and sample frequency offset correction. The top curve shows the performance when an uncorrected sample frequency offset is present.

V. MIMO-OFDM CHANNEL ESTIMATION

Channel state information is required in MIMO-OFDM for space–time coding at the transmitter and signal detection at receiver. Its accuracy directly affects the overall performance of MIMO-OFDM systems. In this section, we present several approaches for MIMO-OFDM channel estimation.

A. Basic Channel Estimation

Channel estimation for OFDM can exploit time and frequency correlation of the channel parameters. A basic channel estimator has been introduced in [31].

As discussed before, for a MIMO system with Q transmit antennas, the signal from each receive antenna at the kth subchannel of the nth OFDM block can be expressed as[1]

$$R_{n,k} = \sum_{q=1}^{Q} H_{n,k}^{(q)} X_{n,k}^{(q)} + W_{n,k}$$

where $H_{n,k}^{(q)}$ is the channel frequency response at the kth subchannel of the nth OFDM block corresponding to the qth transmit antenna, and $W_{n,k}$ is the additive white Gaussian noise. The challenge with MIMO channel estimation is

---

[1]We omit the index for receive antenna here, since channel estimation for each receive antenna is performed independently.
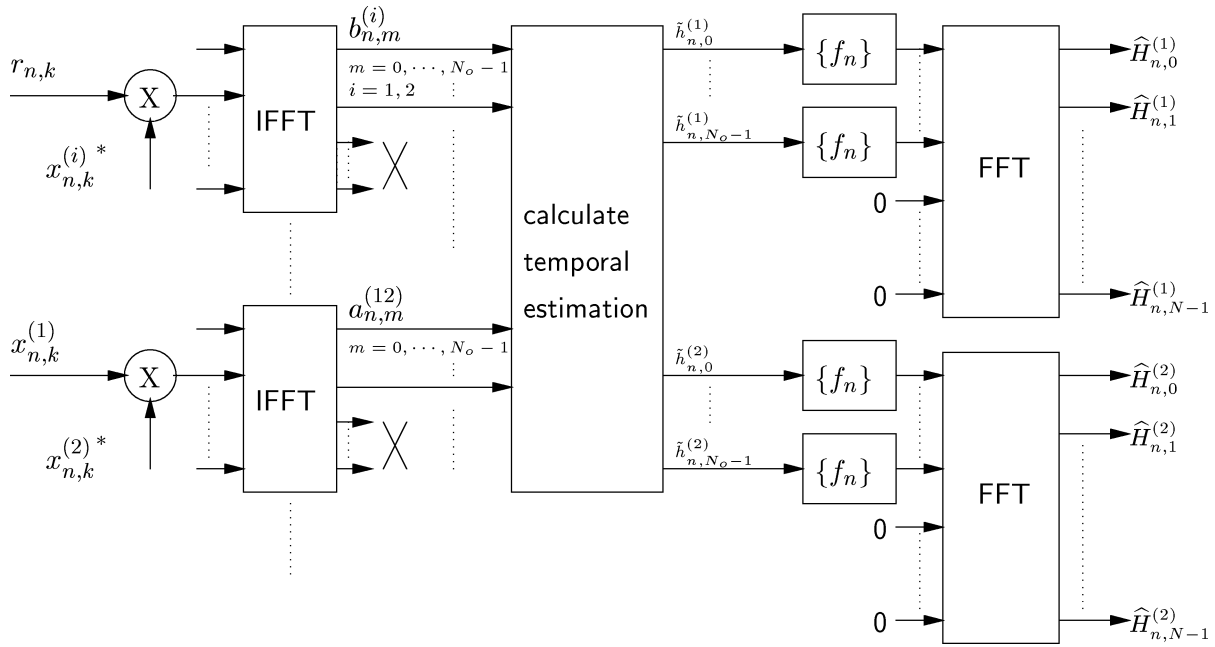
Fig. 7. Basic channel parameter estimator for MIMO-OFDM with two transmit antennas.

that each received signal corresponds to several channel parameters.

Since the channel response at different frequencies is correlated, channel parameters at different subcarriers can be expressed as

$$H_{n,k}^{(q)} = \sum_{m=0}^{N_o-1} h_{n,m}^{(q)} W_N^{km} \qquad (23)$$

for $k = 0, 1, \ldots, N - 1$ and $q = 1, \ldots, Q$. The parameter N_o depends on the ratio of the delay span of wireless channels and the OFDM symbol duration, and $W_N = \exp(-\jmath(2\pi/N))$. Hence, to obtain $H_{n,k}^{(q)}$, we only need to estimate $h_{n,m}^{(q)}$.

If the transmitted signals $X_{n,k}^{(q)}$ from the qth transmit antenna are known for $q = 1, \ldots, Q^2$, then $\tilde{h}_{n,m}^{(q)}$, a temporal estimation of $h_{n,m}^{(q)}$, can be found by minimizing the following cost function:

$$\sum_{k=0}^{N-1} \left| R_{n,k} - \sum_{q=1}^{Q} \sum_{m=0}^{N_o-1} \tilde{h}_{n,m}^{(q)} W_K^{km} x_{n,k}^{(q)} \right|^2. \qquad (24)$$

Direct calculation in [31] yields

$$\begin{pmatrix} \mathbf{A}_n^{(11)} & \cdots & \mathbf{A}_n^{(Q1)} \\ \vdots & \cdots & \vdots \\ \mathbf{A}_n^{(1Q)} & \cdots & \mathbf{A}_n^{(QQ)} \end{pmatrix} \begin{pmatrix} \tilde{\mathbf{h}}_n^{(1)} \\ \vdots \\ \tilde{\mathbf{h}}_n^{(Q)} \end{pmatrix} = \begin{pmatrix} \mathbf{b}_n^{(1)} \\ \vdots \\ \mathbf{b}_n^{(Q)} \end{pmatrix} \qquad (25)$$

or

$$\begin{pmatrix} \tilde{\mathbf{h}}_n^{(1)} \\ \vdots \\ \tilde{\mathbf{h}}_n^{(Q)} \end{pmatrix} = \begin{pmatrix} \mathbf{A}_n^{(11)} & \cdots & \mathbf{A}_n^{(Q1)} \\ \vdots & \cdots & \vdots \\ \mathbf{A}_n^{(1Q)} & \cdots & \mathbf{A}_n^{(QQ)} \end{pmatrix}^{-1} \begin{pmatrix} \mathbf{b}_n^{(1)} \\ \vdots \\ \mathbf{b}_n^{(Q)} \end{pmatrix} \qquad (26)$$

[2]During the training period, transmitted signals are know to the receiver. In the data transmission mode, a decision-directed approach can be used

where $\tilde{\mathbf{h}}_n^{(q)}$ is the temporal estimation of channel parameter vector, defined as

$$\tilde{\mathbf{h}}_n^{(q)} = \left(\tilde{h}_{n,0}^{(q)}, \ldots, \tilde{h}_{n,N_o-1}^{(q)} \right)^T$$

and $a_{n,m}^{(ij)}$, $\mathbf{A}_n^{(ij)}$, $b_{n,m}^{(i)}$, and $\mathbf{b}_n^{(i)}$ are defineded as

$$a_{n,m}^{(ij)} = \sum_{k=0}^{N-1} x_{n,k}^{(i)} x_{n,k}^{(j)*} W_N^{-km} \qquad (27)$$

$$\mathbf{A}_n^{(ij)} = \left(a_{n,m_1-m_2}^{(ij)} \right)_{m_1,m_2=0}^{N_o-1}$$

$$b_{n,m}^{(i)} = \sum_{k=0}^{N-1} r_{n,k} x_{n,k}^{(i)*} W_N^{-km} \qquad (28)$$

and

$$\mathbf{b}_n^{(i)} = \left(b_{n,0}^{(i)}, \ldots, b_{n,N_o-1}^{(i)} \right)^T$$

respectively.

From the temporal estimation of channel parameters, robust estimation can be obtained using the approach developed in [32], which exploits the time correlation of channel parameters. Robust estimation of channel parameter vectors at the nth OFDM block can be obtained by

$$\hat{\mathbf{h}}_n^{(i)} = \sum_{l \geq 0} f_l \tilde{\mathbf{h}}_{n-l}^{(i)}$$

where f_l's ($l \geq 0$) are the coefficients for the robust channel estimator [31], [32].

Fig. 7 illustrates the block diagram of the basic channel estimator for a MIMO-OFDM system with two transmit antennas. To calculate temporal estimation in the figure, a $2N_o \times 2N_o$ matrix inversion is need to get the temporal estimation of $h_{n,m}^{(1)}$ and $h_{n,m}^{(2)}$. In general, a $QN_o \times QN_o$ matrix inversion is required for a MIMO-OFDM system
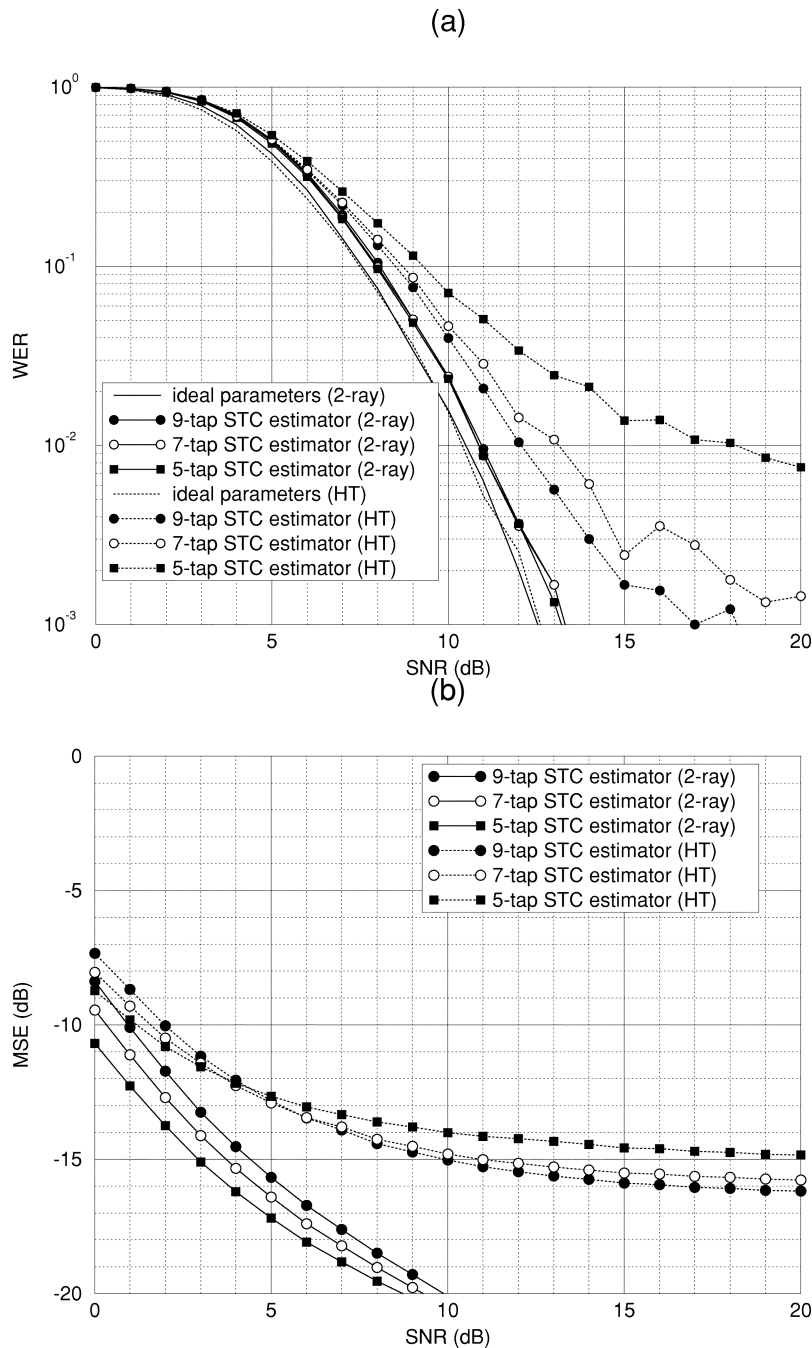
Fig. 8. (a) WER and (b) MSE of a 2 × 2 MIMO-OFDM system when a wireless channel with 40-Hz Doppler frequency and the two-ray and the COST207 HT delay profiles, respectively.

with Q transmit antennas, which is computationally intensive. To reduce the computational complexity, the significant-tap-catching estimator has been proposed in [31].

To study the impact of channel estimation error on MIMO-OFDM performance, a 2 × 2 MIMO-OFDM system with space–time coding is simulated. The parameters of the simulated OFDM system are similar to those in [31] and [32]. The OFDM signal consists of 128 tones, including eight guard tones on each side, and with 160-μs symbol duration. A 40-μs guard interval is used, resulting in a total block length $T_f = 200$ μs and a subchannel symbol rate

$r_b = 5$ kbaud. A 16-state 4-PSK space–time code is used. In brief, the overall system can transmit data at a rate of 1.18 Mb/s over an 800-kHz channel, i.e., the bandwidth efficiency is 1.475 b/s/Hz.

Fig. 8 compares the performance between channels with the two-ray and the COST207 HT delay profiles with $f_d = 40$ Hz. From the figure, the system has the same performance when the ideal parameters of the previous OFDM block are used for decoding. However, when estimated parameters are used, the system has better performance for the two-ray delay profile than for the HT profile, since the estimator has lower MSE for the two-ray delay profile as we

can see from Fig. 8(b). When the seven-tap or nine-tap significant-tap-catching technique in [31] is used, the required SNR for a 10% WER is 8 dB for the two-ray delay profile and and about 8.6 dB for the COST207 HT delay profile, respectively.

B. Optimum Training Sequences for Channel Estimation

In this section, we describe optimum training that can simplify initial channel estimation and optimize estimation performance.

For simplicity, we assume that modulation results in constant-modulus signals, that is, $|x_{n,k}^{(q)}| = 1$. From (27)

$$a_{n,m}^{(ii)} = N\delta[m]$$

where $\delta[m]$ denotes the unit impulse function. Consequently, $\mathbf{A}_n^{(ii)} = N\mathbf{I}$, where $\mathbf{I}$ is a $N_o \times N_o$ identity matrix. If the training sequences $\{x_{1,k}^{(q)}\}$'s are chosen such that $\mathbf{A}_1^{(ij)} = \mathbf{0}$ for $i \neq j$, then, from (26), $\tilde{\mathbf{h}}_1^{(i)} = (1/N)\mathbf{b}_1^{(i)}$, and no matrix inversion is required for channel estimation.

To find $x_{1,k}^{(q)}$ for $q \geq 2$ with $|x_{1,k}^{(q)}| = 1$ and $\mathbf{A}_1^{(ij)} = \mathbf{0}$ for $i \neq j$, it is sufficient to find $a_{1,m}^{(ij)} = 0$ for $|m| \leq N_o - 1$, since $\mathbf{A}_1^{(ij)}$ only consists of $a_{1,m}^{(ij)}$'s for $|m| \leq N_o - 1$, where $m \equiv N + m$ if $m < 0$.

To construct training sequences such that $\mathbf{A}_1^{(ij)} = \mathbf{0}$, let the training sequence for the first antenna $\{x_{1,k}^{(1)}\}$ be any sequence that is *good* for time and frequency synchronization and other properties, such as low PAPR. For a MIMO-OFDM system with the number of transmit antennas, Q, less than or equal to N/N_o, let

$$x_{1,k}^{(q)} = x_{1,k}^{(1)} W_N^{-\bar{N}_o(q-1)k} \tag{29}$$

for $q = 2, \ldots, Q$, where $\bar{N}_o = \lfloor N/Q \rfloor \geq N_o$ and $\lfloor z \rfloor$ denotes the largest integer no larger than z. Then for any $i \leq j$

$$a_{n,m}^{(ij)} = N\delta[m - \bar{N}_o(j-i)]. \tag{30}$$

Note that $1 \leq j - i \leq p - 1$; therefore

$$\bar{N}_o(j-i) \geq \bar{N}_o \geq N_o \tag{31}$$

and

$$\bar{N}_o(j-i) \leq \bar{N}_o(p-1) = \bar{N}_o p - \bar{N}_o \leq N - N_o. \tag{32}$$

Consequently, $a_{1,m}^{(ij)} = 0$ for $0 \leq m \leq N_o - 1$ or $N - N_o + 1 \leq m \leq N - 1$ (equivalent to $|m| \leq N_o - 1$), which results in $\mathbf{A}_1^{(ij)} = \mathbf{0}$ for all $i < j$. If $i > j$, $\mathbf{A}_1^{(ij)} = (\mathbf{A}_1^{(ji)})^H = \mathbf{0}$. Hence, $\mathbf{A}_1^{(ij)} = \mathbf{0}$ for all $i \neq j$.

It should be indicated that the above optimum training sequence design approach is not applicable to those MIMO-OFDM systems with more than N/N_o transmit antennas.

It is proved in [31] that the MSE of the basic temporal channel estimation reaches the low bound when $\mathbf{A}_1^{(ij)} = \mathbf{0}$ for $i \neq j$. Therefore, optimum training sequence can not only reduce the complexity of channel estimation but also improve

the performance of temporal channel parameter estimation during training period.

C. Simplified Channel Estimation

In the above section, we have introduced optimum sequences for channel estimation, which not only improve the initial channel estimation during the training period but also simplify channel estimation. During the data transmission period ($n > 1$), transmitted symbols are random; therefore, we cannot control $\mathbf{A}_n^{(ij)}$. Here, we introduce an approach that simplifies channel estimation during data transmission mode.

From (25), for the nth OFDM block, we have

$$\mathbf{A}_n^{(ii)}\tilde{\mathbf{h}}_n^{(i)} = \mathbf{b}_n^{(i)} - \sum_{j=1, j\neq i}^{Q} \mathbf{A}_n^{(ji)}\tilde{\mathbf{h}}_n^{(i)} \tag{33}$$

for $i = 1, \ldots, Q$. In the above expression, the subscript n has been added to indicate that those vectors and matrices are related to the nth OFDM block. From the discussion in the previous section, for an OFDM system with constant modulus modulation, $\mathbf{A}^{(ii)} = N\mathbf{I}$ for $i = 1, \ldots, Q$, and, therefore

$$\tilde{\mathbf{h}}_n^{(i)} = \frac{1}{N}\left(\mathbf{b}_n^{(i)} - \sum_{j=1, j\neq i}^{Q} \mathbf{A}_n^{(ji)}\tilde{\mathbf{h}}_n^{(i)}\right) \tag{34}$$

for $i = 1, \ldots, Q$. From the above equations, if $\tilde{\mathbf{h}}_n^{(i)}$'s for $j = 1, \ldots, i-1, i+1, \ldots, Q$ are known, then $\tilde{\mathbf{h}}_n^{(i)}$ can be estimated without any matrix inversion.

If robust estimation of channel parameter vectors at previous OFDM block, $\hat{\mathbf{h}}_{n-1}^{(i)}$'s for $i = 1, \ldots, Q$ are used to substitute $\tilde{\mathbf{h}}_n^{(i)}$ on the right side of (34), then

$$\tilde{\mathbf{h}}_n^{(i)} = \frac{1}{N}\left(\mathbf{b}_n^{(i)} - \sum_{j=1, j\neq i}^{p} \mathbf{A}^{(ji)}\hat{\mathbf{h}}_{n-1}^{(j)}\right) \tag{35}$$

for $i = 1, \ldots, Q$, and the matrix inversion in (26) can be avoided.

The simplified channel estimation described above significantly reduces the computational complexity of channel estimation; it may also cause some performance degradation. However, it is demonstrated by theoretical analysis and computer simulation in [33] that the performance degradation is negligible.

D. Enhanced Channel Estimation

In [31] and [33] (Sections V-A–V-C), we have introduced channel parameter estimators and optimum training sequences for OFDM with multiple transmit antennas. Furthermore, for a MIMO-OFDM system where many independent channels with the same delay profile are involved, the channel delay profile can be more accurately estimated. By exploiting the estimated channel delay profile, channel parameter estimation can be further improved.

From the above discussion, for the nth OFDM block, channel parameters corresponding to the qth transmit and the lth receive antenna pairs, $h_{n,m}^{(ql)}$ in (23), can be estimated
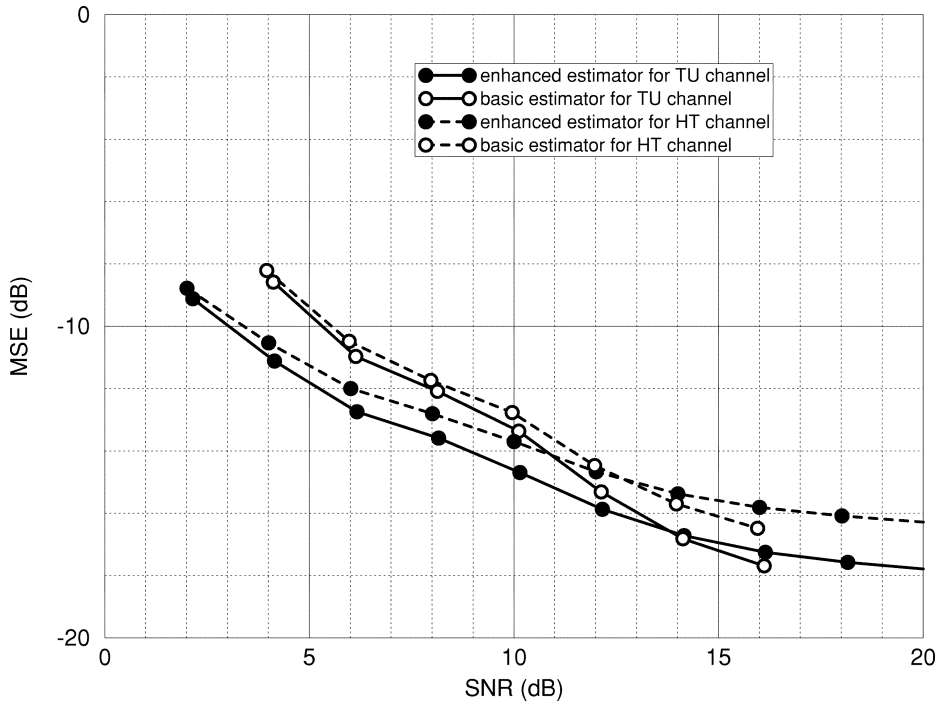
Fig. 9. MSE comparison of the basic and the enhanced channel estimation techniques for a 4×4 MIMO-OFDM system.

using the correlation of channel parameters at different times and frequencies. With $\hat{h}_{n,m}^{(ql)}$, the estimated $h_{n,m}^{(ql)}$, the channel frequency response at the kth tone of the nth OFDM block can be reconstructed by

$$\hat{H}_{n,k}^{(q,l)} = \sum_{m=0}^{N_o-1} \hat{h}_{n,m}^{(q,l)} W_N^{km}. \tag{36}$$

The estimated channel parameter, $\hat{h}_{n,m}^{(q,l)}$, can be decomposed into the true channel parameter, $h_{n,m}^{(q,l)}$, and an estimation error, $e_{n,m}^{(q,l)}$, that is

$$\hat{h}_{n,m}^{(q,l)} = h_{n,m}^{(q,l)} + e_{n,m}^{(q,l)}. \tag{37}$$

From [33], $e_{n,m}^{(q,l)}$ can be assumed to be Gaussian with zero-mean and variance σ^2, and independent for different qs, ls, ns, or ms. If the parameter estimation quality is measured by means of the normalized MSE (NMSE), which is defined as

$$\text{NMSE} = \frac{E\left|\hat{H}_{n,k}^{(q,l)} - H_{n,k}^{(q,l)}\right|^2}{E\left|H_{n,k}^{(q,l)}\right|^2}$$

then it can be calculated directly that the NMSE for the estimation in (36) is

$$\text{NMSE}_r = N_o \sigma^2 \tag{38}$$

where we have used the assumption that

$$\sum_{l=0}^{N_o-1} E\left|h_{n,m}^{(q,l)}\right|^2 = \sum_{l=0}^{N_o-1} \sigma_m^2 = 1$$

with $\sigma_m^2 = E\left|h_{n,m}^{(q,l)}\right|^2$.

If the channel's delay profile, that is, σ_m^2's for $m = 0, \ldots, N_o - 1$, is known, and it can be used to reconstruct the channel frequency response from $\hat{h}_{n,m}^{(q,l)}$, the NMSE of $\hat{H}_{n,k}^{(q,l)}$ can be significantly reduced. In this case, if the α_m's are selected to minimize the NMSE of

$$\hat{H}_{n,k}^{(q,l)} = \sum_{m=0}^{N_o-1} \alpha_m \hat{h}_{n,m}^{(q,l)} W_N^{km} \tag{39}$$

then it can be proven that the optimal α_m is

$$\alpha_m = \frac{\frac{\sigma_m^2}{\sigma_m^2 + \sigma^2}}{\sum\limits_{m'=0}^{N_o-1} \frac{\sigma_{m'}^4}{\sigma_{m'}^2 + \sigma^2}} \tag{40}$$

and the NMSE is

$$\text{NMSE}_o = \frac{\sigma^2 \sum\limits_{m=0}^{N_o-1} \frac{\sigma_m^2}{\sigma_m^2 + \sigma^2}}{\sum\limits_{m=0}^{N_o-1} \frac{\sigma_m^4}{\sigma_m^2 + \sigma^2}}. \tag{41}$$

As indicated in [32], channel's delay profile depends on the environment and, therefore, is usually unknown. However, for MIMO-OFDM systems, channels corresponding to different transmit or receive antennas should have approximately the same delay profile. Therefore, $\sigma_m^2 = E\left|h_{n,m}^{(q,l)}\right|^2$ can be estimated by

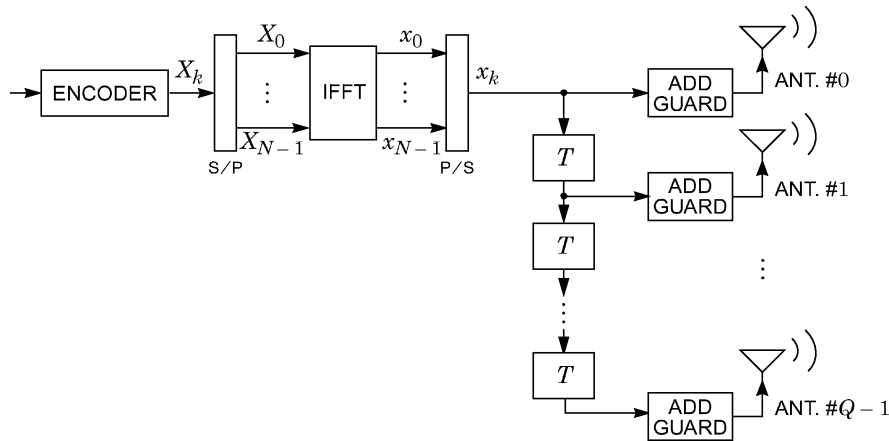$$\hat{\sigma}_m^2 = \frac{1}{QL} \sum_{q=1}^{Q} \sum_{l=1}^{L} \left|\hat{h}_{n,m}^{(q,l)}\right|^2.$$

Fig. 10. A multicarrier delay-diversity modulation (MDDM) transmitter.

With the estimated σ_m^2, enhanced channel frequency responses can be reconstructed by (39).

Fig. 9 compares the MSE of the basic and enhanced channel estimation for a 4×4 MIMO-OFDM system. From the figure, the MSE of the enhanced channel estimator is about 1.5 dB better for the COST207 TU channels and 1 dB better for the COST207 HT channels than the basic estimator described in Section V-A and [31].

VI. Space–Time Coding Techniques for MIMO-OFDM

OFDM is an effective and low-complexity strategy for dealing with frequency-selective channels. Roughly speaking, an OFDM transmitter divides the frequency band into N narrow subchannels and sends a different sequence of symbols across each subchannel. When the subchannel bandwidth is sufficiently narrow, the frequency response across each subchannel is approximately flat, avoiding the need for complicated time-domain equalization. In this way, OFDM transforms a frequency-selective channel into a collection of N separate flat-fading channels. In the same way, when an OFDM transmitter is used by each of Q transmit antennas, and an OFDM front-end is used by each of L receive antennas, a MIMO frequency-selective channel is transformed into a collection of N flat-fading MIMO channels, one for each tone, with each having dimension $L \times Q$.

Traditional space–time codes were designed to extract spatial diversity from a flat-fading MIMO channel, and are not generally effective at extracting the additional *frequency* (or multipath) diversity of a frequency-selective fading channel. Quantitatively, the maximum achievable diversity order is the product of the number of transmit antennas, the number of receiver antennas, and the number of resolvable propagation paths (i.e., the channel impulse response length) [11], [12]. To achieve this full diversity requires that the information symbols be carefully spread over the tones as well as over the transmitting antennas. A *space-frequency* code—or more generally, a space–time-frequency code—is a strategy for mapping information symbols to antennas and tones as a means for extracting both spatial and frequency diversity.

Space-frequency codes based directly on space–time codes (with time reinterpreted as frequency) have been proposed [10], [19], [50]–[52], but they fail to exploit the frequency diversity of a frequency-selective fading MIMO channel [11]. Guidelines for the design of full-diversity space-frequency codes are given in [11]. A simple method for transforming any full-diversity space–time code into a full-diversity space-frequency code has recently been proposed, at the expense of a reduced rate [49]. An example of a space-frequency code that achieves full spatial and frequency diversity is given in [13]. The design of space-frequency and space–time-frequency codes is currently an active area of research [11]–[18].

In the remainder of this section we highlight two approaches to space–time processing for MIMO-OFDM. The first is a combination of delay-diversity and OFDM known as multicarrier delay-diversity modulation, while the second is a closed-loop system with channel knowledge at the transmitter.

A. Multicarrier Delay Diversity Modulation

Delay diversity was the first transmit diversity approach for flat-fading MIMO channels [34]–[37]. Multiple transmit antennas send delayed copies of same signal, and maximum-likelihood sequence estimation [36], [38] or decision-feedback equalization [39] is used at the receiver to estimate the transmitted sequence. The natural ability of OFDM to mitigate frequency-selective fading makes delay diversity an attractive option for MIMO-OFDM [20]. For frequency-selective fading channels, a cyclic delay-diversity approach with OFDM is proposed in [21], a combination known as *multicarrier delay-diversity modulation (MDDM)*. MDDM is further investigated with space–time block coding in [22]. With proper coding, MDDM can achieve full spatial diversity on flat fading channels [23]. Moreover, MDDM provides a very flexible space–time coding approach for any number of transmit antennas, allowing the number of transmit antennas to be changed without changing the codes that are employed, unlike STBC [23].

Fig. 10 shows the baseband MDDM transmitter with Q transmit antennas. A length-N sequence $(X_0, \ldots, X_{N-1})$
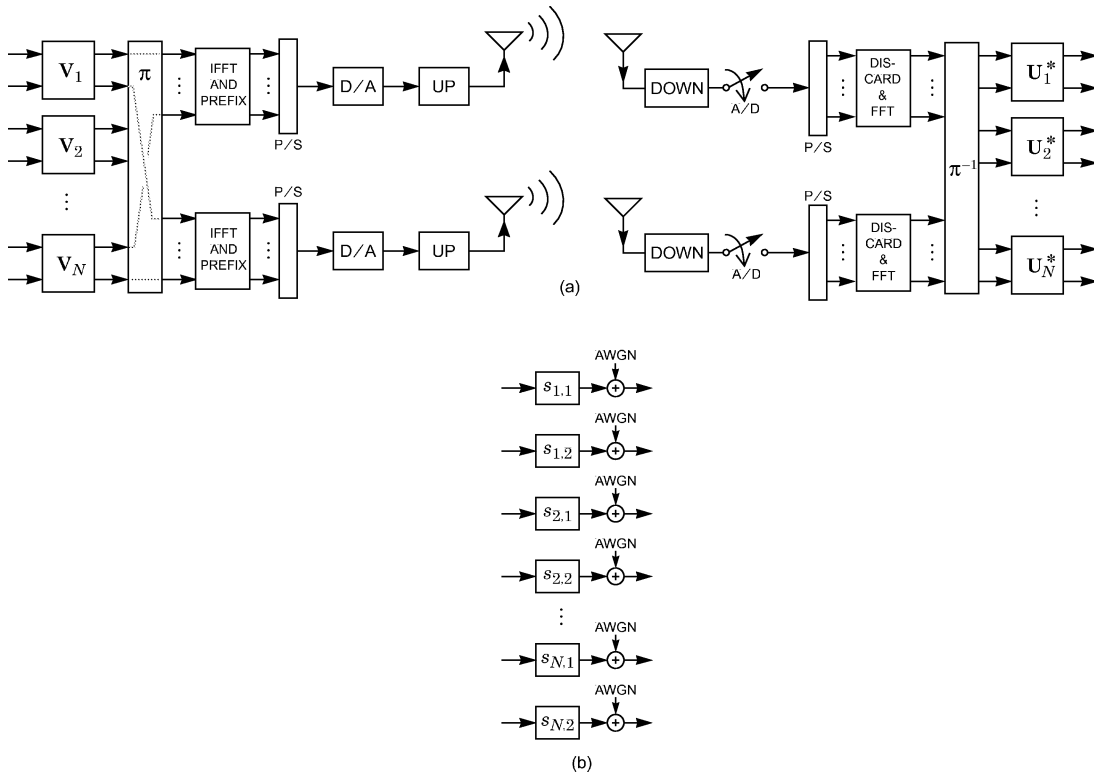
Fig. 11. A combination of eigenbeamforming and OFDM transforms a closed-loop frequency-selective fading channel: (a) into a bank of scalar channels and (b) each with independent noise.

modulates N subcarriers, where the multicarrier modulation is, again, an IDFT. A length-G cyclic guard interval in the form of a CP is added to the time domain sequence $\{x_n\}$. The Q transmit antennas are arranged in a length-Q tapped-delay line configuration, where the delay interval is equal to symbol period T of the sequence $\{x_n\}$. The initial values of transmitting antennas are $x_{N-G}, x_{N-G-1}, \ldots, x_{N-G-Q+1}$ for the zeroth antenna to the $(Q-1)$th antenna, respectively. The MDDM scheme uses cyclic delay diversity and, therefore, does not require an increase in the guard interval to account for the cyclic delays of the transmitter.

Consider MDDM with Q transmit antennas and transmitted sequences $\mathbf{X}$ of length N, $N > Q$. Note that $\mathbf{X}$ is the encoded sequence in the frequency domain before the IDFT. If all distinct pairs of sequences $(\mathbf{X}, \tilde{\mathbf{X}})$, $\mathbf{X} \neq \tilde{\mathbf{X}}$ differ in at least Q coordinates, then MDDM achieves full spatial diversity on quasistatic flat Rayleigh fading channels [23]. For BPSK and QPSK symbols this give a simple design criteria: any binary code $\mathcal{C}$ having minimum distance $d_m \geq Q$ will achieve full spatial diversity for an MDDM system having Q-transmit antennas. With MDDM, interleaving of the coded bits is also necessary for maximizing the coding gain. Criteria for *optimum* interleaving have been derived in [23], where it is also shown that a simple block interleaver achieves near optimum performance.

B. Closed-Loop MIMO-OFDM

A *closed-loop* MIMO transmitter has knowledge of the channel, allowing it to perform an optimal form of precompensation at the transmitter known as *eigenbeamforming*. In particular, for a flat-fading channel, it is well known that a capacity-achieving transmitter bases its space–time processing on an SVD of the $L \times Q$ matrix of channel gains $\mathbf{H} = \mathbf{USV}^*$, where $(\cdot)^*$ denotes the Hermitian transpose, where $\mathbf{U}$ and $\mathbf{V}$ have orthogonal columns, and where $\mathbf{S}$ is a diagonal matrix whose diagonal entries are the nonnegative singular values that are ordered from largest to smallest. A capacity-approaching transmitter will then implement eigenbeamforming by applying the linear filter $\mathbf{V}$ to symbol vectors before transmission. A receiver matched to the cascade of this prefilter and the channel will essentially apply the filter $\mathbf{U}^*$ to the received vector, which transforms the flat-fading channel into a bank of independent scalar channels. The problem has, thus, been reduced to one of communication across a bank of independent parallel scalar subchannels, where the subchannel gains are the nonnegative, nonincreasing singular values of the channel.

Because OFDM reduces a frequency-selective channel to a collection of flat-fading MIMO channels, a closed-loop MIMO-OFDM system can use eigenbeamforming on a tone-by-tone basis to transform a frequency-selecting MIMO channel into a collection of MN parallel subchannels [9], where $M = \min\{Q, L\}$ is the minimum number of antennas at each end and N is the number of OFDM tones. A MIMO-OFDM system with eigenbeamforming is illustrated in Fig. 11(a) for the special case of two transmit and two receive antennas. The prefilters $\{\mathbf{V}_n\}$ and postfilters $\{\mathbf{U}_n^*\}$ are related to the 2-by-2 matrix of channel gains for the

nth tone $\mathbf{H}_n$ by the SVD $\mathbf{H}_n = \mathbf{U}_n \mathbf{S}_n \mathbf{V}_n^*$. The permuter π at the transmitter is a simple row-column interleaver of dimension $N \times 2$. The entire system of Fig. 11(a) reduces to the bank of scalar channels shown in Fig. 11(b), where $s_{i,j}$ denotes the ith singular value for the jth tone.

Ideally, information bits (constellation size) and symbol energy would be allocated to the MN subchannels of Fig. 11(b) so as to minimize the overall SNR requirement, subject to a target bit rate. (Alternatively, the bits and energy could be allocated so as to maximize the bit rate, subject to a target energy constraint.) Unfortunately, the complexity of an exhaustive search for the bit-allocation is prohibitive when the number of subchannels is large. In a practical MIMO-OFDM application, the number of subchannels MN can be very large, which motivates a search for low-complexity bit-allocation strategies with near-optimal performance.

A simple and effective way to reduce complexity is to impose a *flat-frequency constraint*, where each tone is restricted to have the same rate budget [40]. We now illustrate that the penalty due to this constraint can be small. Let B denote the total rate budget for each OFDM signaling interval. Without the flat-frequency constraint, and without constraining the symbols to a discrete alphabet, the optimal rate $r_{i,j}$ for the ith spatial channel (singular value) and the jth tone is found by waterpouring over both space and frequency, yielding

$$r_{i,j} = \{\log_2(\lambda s_{i,j}^2)\}^+$$

where $\{x\}^+ = \max\{0, x\}$, and where λ ensures that the total rate budget is met $\sum_{i,j} r_{i,j} = B$. On the other hand, if we enforce the flat-frequency constraint, the constrained optimal solution is

$$r_{i,j} = \{\log_2(\mu_j s_{i,j}^2)\}^+$$

where μ_j ensures that $\sum_i r_{i,j} = B/N$ for each $j = 1, \ldots N$. Since μ_j is calculated anew each tone, this amounts to water pouring over space but not frequency. In either case, the average required SNR is given by

$$\frac{E}{N_0} = E\left[\sum_{i=1}^{M}\sum_{j=1}^{N}\frac{2^{r_{i,j}} - 1}{s_{i,j}^2}\right]$$

which serves as a figure of merit.

The penalty of the flat-frequency constraint is easily measured by comparing this SNR requirement with and without the constraint. For example, Fig. 12 illustrates the SNR penalty of the flat frequency as a function of zero-outage capacity, also known as the delay-limited capacity, in bits per second per hertz. These results were based on 10 000 independent frequency-selective channels generated according to a five-path equal-power profile, with Rayleigh fading on each path. The SNR penalty for the case of a 2×2 channel ($M = 2$) is relatively large, about 1.0 dB. However, for the cases of $M = 4$ and $M = 6$, the flat-frequency strategy performs only marginally worse, suffering a 0.1-dB penalty for $M = 4$ and a 0.05 dB penalty for $M = 6$. Clearly,
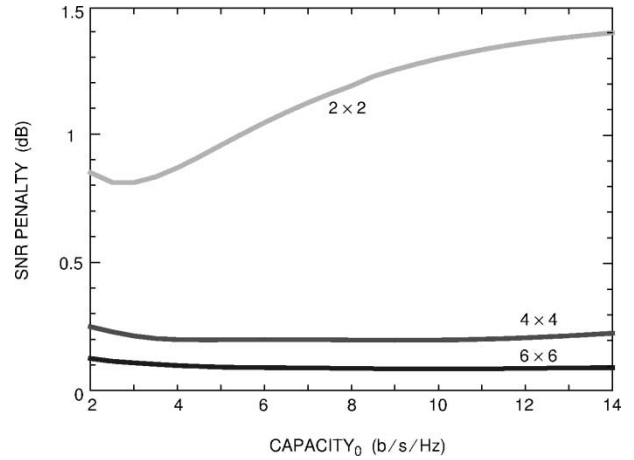

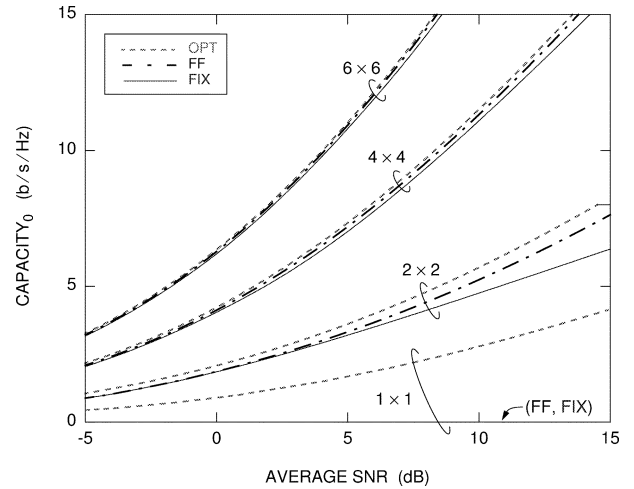**Fig. 12.** The flat-frequency constraint incurs a small SNR penalty.

Fig. 13. The nonadaptive (FIX) strategy, which uses a combination of the flat-frequency (FF) constraint and a fixed spatial allocation, approaches the fully adaptive waterpouring solution as the number of antennas grows.

the flat-frequency constraint incurs little penalty, especially when there are more than two antennas at each end.

We can further reduce complexity by imposing a *fixed spatial allocation* on top of the flat-frequency constraint [41]. Instead of exhaustively searching all possible spatial allocations meeting a bit budget of B/N, this strategy fixes the allocation based on the anticipated statistics of MIMO Rayleigh fading channels. The penalty due to a fixed allocation is surprisingly small, thanks to a combination of the known Rayleigh fading statistics and the asymptotic nonrandomness of the singular values. Combining the flat-frequency constraint with a fixed spatial allocation per tone leads to a totally *nonadaptive* rate-allocation strategy. Remarkably, this fixed-frequency fixed-space strategy performs reasonably well when there are two antennas at each end, and it is even better when there are more antennas.

Fig. 13 illustrates the performance of the nonadaptive strategy with the water-pouring solution, with and without the flat-frequency constraint. The channel conditions are identical to those used in Fig. 12. Although the nonadaptive strategy suffers a significant penalty when $M = 2$, it is

nearly optimal for for $M = 4$ and $M = 6$. The conclusion is that a closed-loop MIMO system need not perform adaptive modulation in order to approach capacity. Instead, a combination of eigenbeamforming and fixed modulation is sufficient, at least on independent identically distributed (i.i.d.) Rayleigh channels with more than two antennas at each end.

VII. ERROR CORRECTION CODING FOR MIMO-OFDM

There are many possible error control strategies in MIMO-OFDM systems. In this section we highlight some of the methods that have been proposed. At this writing this is a very active and rapidly evolving research area. As in any system there are important performance-complexity tradeoffs; however, we do not address those here. Furthermore, depending on the application, the desired BER may result in the need for only minimal or no error correction; namely, the modulation code might be sufficient to provide the needed BER, for example, 10^{-3}. However, if either near capacity performance or a very low BER is required (e.g., 10^{-6} to 10^{-12}), a powerful error control code is needed. From this perspective much of the recent work has focused on the use of iteratively decodable codes such as turbo codes and low-density parity check (LDPC) codes. As turbo codes are special cases of LDPCs, we focus on those. Also, we start our description with single-input single-output (SISO) channels as many practical error control strategies for MIMO systems will be designed for SISO channels and then mapped to MIMO channels.

A. LDPCs and SISO Flat Fading Channels

LDPCs are specified by a sparse parity-check matrix and can be categorized into regular and irregular LDPC codes. The regular LDPC codes have parity-check matrices whose columns have the same number of ones. In this paper, we focus on regular LDPC codes.

A parity-check matrix $\mathbf{P}$ of a (c, t, r) LDPC code has c columns, t ones in each column, and r ones in a row. A (c, t, r) LDPC code has a code rate of $1 - t/r$. Gallager [42] showed that there is at least one LPDC code whose minimum distance $d_{\min}$ grows linearly with block length c when $t > 2$. Therefore, we can expect a better coding gain with a longer code length, although the coding length is limited by practical considerations like decoding latency, decoder complexity, etc. The rate of growth of $d_{\min}$ is bounded by a nonzero number, which is determined by the selection of t and r.

The belief propagation algorithm has been widely adopted for decoding LDPC codes. MacKay [43] gives a good description of the iterative message passing decoder based on the belief propagation algorithm which can be implemented in either probability or log-probability domain. The decoder in this paper works in the log-probability domain. For the message-passing decoder, we need the LLR of each bit. A general form of the LLR computing formula is given by

$$\text{LLR}(b_j) = \log \left[\frac{\sum_{i=1}^{2^{k-1}} P(\mathbf{R}|b_j = 1, \mathbf{m}_j = m_i)}{\sum_{i=1}^{2^{k-1}} P(\mathbf{R}|b_j = 0, \mathbf{m}_j = m_i)} \right] \quad (42)$$

where $\mathbf{R}$ is a received signal vector, b_j is jth bit of a transmitted message, $\mathbf{m}_j$ is a message less the jth bit, m_i is one of 2^{k-1} possible symbols of $\mathbf{m}_j$, and each symbol carries k bits.

On an AWGN channel with flat fading, (42) can be expressed as

$$\text{LLR}(b_j) = \log \left[\frac{\sum_{i=1}^{2^{k-1}} \exp\left\{ -\frac{d(\mathbf{R}, \mathbf{c}_i^{b_j=1})^2}{2\sigma^2} \right\}}{\sum_{i=1}^{2^{k-1}} \exp\left\{ -\frac{d(\mathbf{R}, \mathbf{c}_i^{b_j=0})^2}{2\sigma^2} \right\}} \right] \quad (43)$$

where $\mathbf{c}_i^{b_j=b}$ is a signal constellation for a message defined by m_i and b_j and $d(\mathbf{R}, \mathbf{c}_i^{b_j=b})$ is the Euclidean distance between the received signal vector $\mathbf{R}$ and $\mathbf{c}_i^{b_j=b}$.

To prevent possible underflow or overflow, the equation can be modified to a more applicable form as

$$
\begin{aligned}
&\text{LLR}(b_j) \\
&= \frac{\left(d_{\min}^0(j)\right)^2 - \left(d_{\min}^1(j)\right)^2}{2\sigma^2} \\
&\quad + \log\left[1 + \sum_{\substack{i=1, \\ i \neq l_1}}^{2^{k-1}} \exp\left\{ -\frac{d(\mathbf{R}, \mathbf{c}_i^{b_j=1})^2 - \left(d_{\min}^1(j)\right)^2}{2\sigma^2} \right\} \right] \\
&\quad - \log\left[1 + \sum_{\substack{i=1, \\ i \neq l_0}}^{2^{k-1}} \exp\left\{ -\frac{d(\mathbf{R}, \mathbf{c}_i^{b_j=0})^2 - \left(d_{\min}^0(j)\right)^2}{2\sigma^2} \right\} \right]
\end{aligned}
\quad (44)
$$

where $d_{\min}^b(j) = d(\mathbf{R}, \mathbf{c}_{l_b}^{b_j=b}) = \min_{1 \leq i \leq 2^{k-1}} d(\mathbf{R}, \mathbf{c}_i^{b_j=b})$ and b is in $\{0, 1\}$.

Fig. 14 shows the BER performance of LDPC codes having code length $c = 1024$ and code rates of 0.5, 0.75, 0.875, and 1.0 (uncoded) with 16 and 64-QAM modulation on an AWGN channel.

Other recent work in this area shows several things regarding the possible *universality* of LDPC codes on fading channels. If the encoder side has partial or full channel knowledge the code rate can be adapted to account for the quality of the channel (provided the fading is slow enough). In [44] it is shown that a properly designed LDPC can be punctured to produce a (higher rate) code that is just a good as an optimally designed code for that higher rate. In principle this allows one to design and implement a single LDPC that is optimal across a range of rates.

If no information is available at the encoder and the fading is faster, other recent work by [45] indicates that a properly designed LDPC might also be universal. That is, regardless
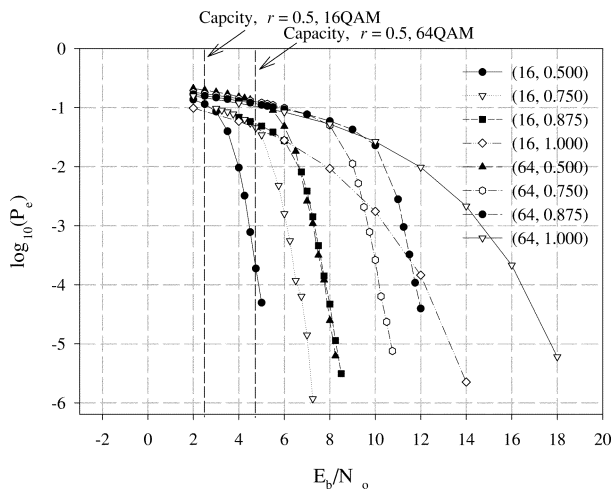
Fig. 14. BER performance of LDPC codes having code length $c = 1024$ and code rates of 0.5, 0.75, 0.875, and 1.0 (uncoded) with 16 and 64-QAM on an AWGN channel.

of the fading, they show that the maximum achievable rate of an LDPC code is very close to the theoretical maximum achievable rate of any code. This indicates that a significantly better code than an LDPC probably does not exist.

Both of these topics are very active and we expect new results that will further strengthen the idea that LDPCs are good both theoretically and practically.

B. SISO and MIMO Channels With and Without OFDM

When a SISO or MIMO channel uses OFDM there are many FEC options. For closed-loop SISO OFDM channels where the encoder has complete channel knowledge (see Section VI-B), a waterfilling approach can be used, where each subcarrier is coded separately at a rate $R_i = \log_2(1 + (|a_i|^2 E_i/2\sigma^2))$. This can be a costly approach if the number of subcarriers is large, since each carrier uses a separate encode and decoder. In systems like IEEE 802.11a, where the encoder does not know the channel, a single (convolutional) code is used across all subcarriers and various decoding strategies can be employed to account for the fact that some subcarriers are better than others. Another case of interest is single-carrier MIMO channel, there are a host of recent papers; see, for example, [46]–[48]

For full MIMO-OFDM, in [53] the LDPC system is compared with space–time trellis code (STTC); the LDPC-based STC can significantly improve the system performance by exploiting both the spatial diversity and the selective-fading diversity in wireless channels. Compared with the recently proposed turbo-code-based STC scheme [54], LDPC-based STC exhibits lower receiver complexity and more flexible scalability.

VIII. ANTENNA AND BEAM SELECTION

The cost of the MIMO-OFDM system is largely driven by the number of transmit and receive chains, for example, each receiver chain includes frequency conversion, IF filtering, and analog-to-digital conversion. The circuits performing these functions must be replicated L times if a MIMO

receiver has L receive branches. However, it is possible to have the spatial diversity and interference suppression benefits of many more antennas than full receiver chains through the use of antenna or beam selection. In this section, we consider antenna and beam selection, give a summary of a low-complexity selection algorithm for OFDM, and show some results for measured channels that compare antenna to beam selection.

A. Antenna Selection

Transmit antenna selection for MIMO has been previously considered for flat-fading MIMO links in the absence of interference [55], [56] and with interference [57], [58]. In the no-interference works, the selection criterion was based on average SNR criteria. Three-select-two antenna selection appeared to give a second-order diversity gain for zero-forcing spatial multiplexing receivers, and produced vector symbol error rates that matched that of the 2 by 2 maximum likelihood receiver without selection [55]. For space–time block coding, selection of two transmit antennas from five to ten antennas, assuming two receive antennas, provided an SNR gain of 2 to 3 dB [56]. For the flat-fading channel with interference, Blum and Winters [57] show about a 7-dB improvement for 8-select-2 diversity at both ends of the link, assuming one or two interference data streams and simulated i.i.d. MIMO channels.

The MIMO selection diversity gain comes with a price: the switch that performs the antenna selection requires a nontrivial design and has a nonnegligible insertion loss [59]. For example the 8-select-2 switch in [59] has an insertion loss of 3.15 dB. In a transmitter, the insertion loss reduces the radiated power. In a receiver, the insertion loss degrades the SNR. The degradation can be made negligible by placing low-noise amplifiers between the antenna elements and the switch. However, this addition can add significant expense to the receiver. On the other hand, the degradation in SNR may not be important if the receiver performance is limited by interference.

The gain from antenna selection for OFDM-MIMO may not be as large as it is for the flat-fading channel because the best selection of elements is likely to change with frequency. While subcarrier-dependent antenna selection is considered in [60], we do not consider this here, since our goal is for the solution to have a certain limited number of transmit and receive chains.

B. Beam Selection

An alternative selection approach for OFDM-MIMO is to select beams instead of selecting antennas. Fig. 15 shows antenna selection (top) and beam selection (bottom) architectures, both incorporating 4-select-2 switches. Beam selection is motivated by the observation that multipath angles are often clustered [61], [62]. The cluster angles are not expected to be very frequency dependent, so the best selection of beams should not change much with frequency. Therefore, if the beamwidth can be matched to the cluster width, there should be an SNR advantage in the absence of interference [63] and a signal-to-interference (SIR) advantage with
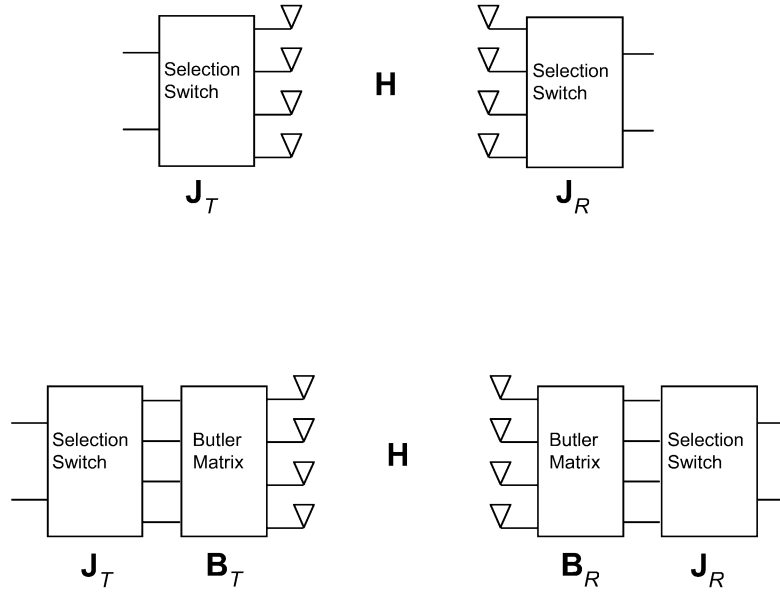
Fig. 15. Antenna selection and beam selection architectures.

interference. Moreover, analog beamforming circuits, such as the Butler matrix [64], are inexpensive compared to the switch at microwave frequencies because they can be implemented in stripline [65]. Therefore, the percentage increase in cost to have beam selection should be small. Like the switch, the beamformer has an insertion loss (2.26 dB for the eight-beam Butler matrix in [65]) so its effects must be more than overcome to justify its use. Two-beam selection for array receivers over simulated clustered indoor channels have indicated that four eight-element linear arrays, placed end to end in a square configuration to provide 360° azimuth coverage, yield an almost 6-dB SNR improvement compared to two fixed omnidirectional antennas when the two beams are processed by a joint decision-feedback equalizer [66]. When the same beam-selection configuration is simulated for space–time block-coded OFDM, an SNR improvement of approximately 5 dB is obtained without interference, and an SIR improvement of more than 16 dB is obtained with interference [67].

C. A Selection Algorithm

In order to select receive beams with good SIR, but with a constraint on the number of full receiver chains, a two-metric, iterative selection algorithm has been proposed [67]. This algorithm assumes a single-input multiple-output channel and it applies to both antenna and beam selection. It is described below for the case of two receiver chains, however, it easily extends to an arbitrary number of receiver chains.

The first metric, the radio signal strength indicator (RSSI), is measured for all beams by analog detectors, while the second metric, the peak-to-trough ratio (PTR) [68], is based on a sliding correlation of the received preamble with one stored OFDM preamble symbol and is computed in the digital signal processor (DSP) prior to full OFDM synchronization. We note that the second metric in [67] is BER. The

PTR, to be defined below, is judged to be a more practical and readily available second metric. The two beams having the highest RSSI are connected to the receiver chains by the RF switch. Then, the PTR values are checked for the two selected beams. If the PTR value for a beam is less than a threshold (which can be set based on the real system's requirement), we conclude that this beam has too much interference; then we check the beam with the next-highest RSSI until we find a PTR value that is higher than the threshold.

To get the PTR value, we use the following equation:

$$R_x(m) = \frac{\left| \sum_{n=0}^{N1} \bar{r}_x(n+m)\bar{t}_x{}^*(n) \right|}{\left| \sum_{n=0}^{N1} \bar{r}_x(n+m)\bar{r}_x{}^*(n+m) \right|} \quad m=0,1,2\ldots.N2 \tag{45}$$

where r_x is the received short training sequence, which includes noise and interference, and t_x is the original one-period-long training sequence. $N1$ is the length of one period of the training sequence. $N2$ is the length of the whole short training sequence plus one period length. $R_x(m)$ is the normalized cross-correlation function. If the received signal includes limited noise and interference, $R_x(m)$ will have $N2/N1 - 1$ peaks. Then each peak and some points on each side of it are removed. The remainder depends on the correlation of the training sequence with the noise and interference. The second metric is computed as

$$PTR = \frac{\langle (\text{magnitude of the peaks})^2 \rangle}{\langle (\text{magnitude of the remainder})^2 \rangle} \tag{46}$$

where $\langle \rangle$ indicates a time average.

Fig. 16 shows the results of a wired hardware test of the PTR metric. The preamble, which is 64 symbols long, is generated at IF. The IF signal was added to the output of a noise generator using a power combiner and then sampled and downconverted. The PTR metric was computed in the DSP.
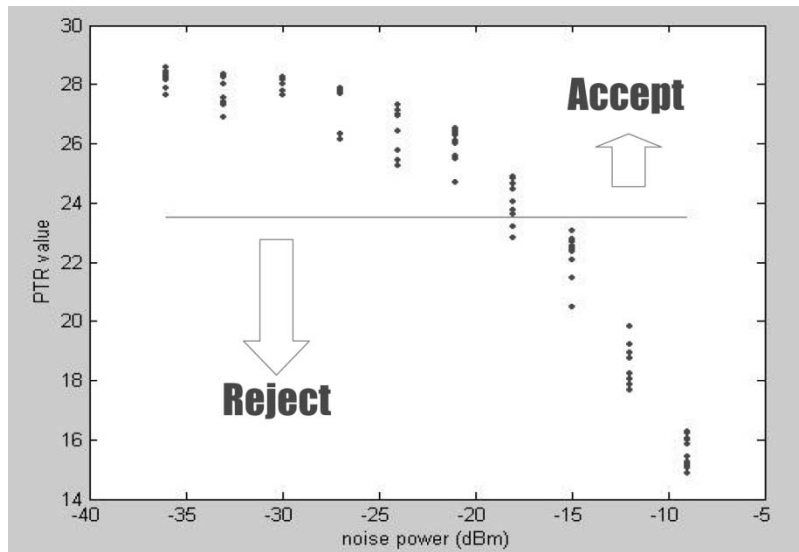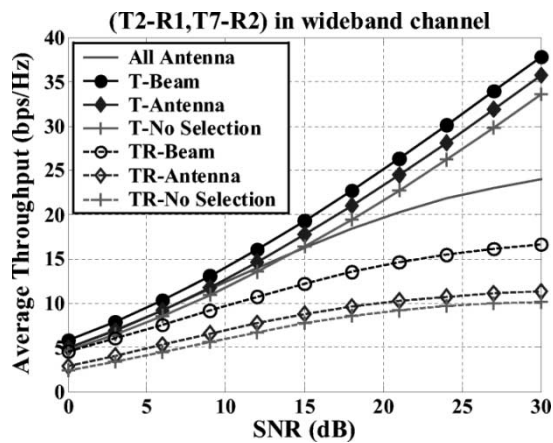
Fig. 16. PTR with different noise powers.

Fig. 17. Average throughput for two interfering MIMO links with various kinds of selection; uncorrelated interference.
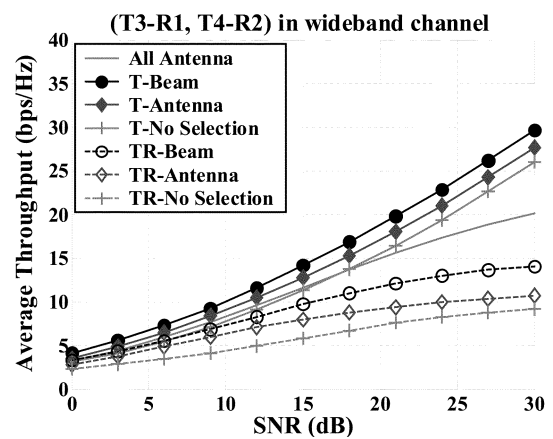

Fig. 18. Average throughput for two interfering MIMO links with various kinds of selection; correlated interference.

Varying amounts of noise were added. The PTR was computed for ten trials for each noise value. The sample values of the PTR metric for each noise power value are shown in Fig. 16. An example beam reject threshold is shown. The figure shows that the PTR is an effective indicator of SNR.

From simulation, we can also conclude that PTR metric is very robust to synchronization offsets: frequency offset, sampling frequency offset, and frame time offset [68].

D. Comparison of Antenna and Beam Selection

The two architectures in Fig. 15 have been compared over indoor MIMO channels measured in the Residential Laboratory (ResLab) at the Georgia Institute of Technology [69]. Using a virtual array approach, four wideband 4×4 MIMO realizations were captured. Each of these realizations was sampled at 51 frequencies, with 10 MHz separation between consecutive frequency samples. Interference was created by a second MIMO link in the ResLab. The performance for each link was quantified by the capacity of the interference-whitened channel, averaged over the 51 frequency samples. The throughput is the sum of these two average capacities. Fig. 17 shows the results for a topology where

the angles of arrival (and departure) of the interference and desired signal are not close, and Fig. 18 corresponds to a topology where both desired and interfering signals are emerging from a hallway, and are, therefore, likely to be close (spatially correlated) [69]. "T-Beam," "T-Antenna," and "T-No Selection" correspond to two transmit beams selected from four, two transmit antennas are selected from four, and the first two transmit antennas are always used, respectively. This corresponds to a condition of "stream control" where neither receiver is overloaded with too many streams [70]. T-beam and T-antenna selection occurs optimally for both interfering links. "TR-Beam," "TR-Antenna," and "TR-No Selection" correspond to the selection occuring at transmitters and receivers. We note that the receivers are overloaded with too many streams for the TR cases. The "All antennas" case has no selection and also corresponds to an overloaded condition. We observe that there is little difference between beam-, antenna-, and no-selection when the receivers are not overloaded for either correlated or uncorrelated interference. However, when the receivers are overloaded, beam selection outperforms antenna selection

for uncorrelated interference by a SNR margin that is 10 dB and larger, depending on the throughput value. The margin is smaller for correlated interference.

IX. MEDIUM ACCESS CONTROL

Although not the focus of this paper, MAC protocols are essential for effective broadband wireless access. MAC protocols for OFDM can be based on time division multiple access (TDMA), where all the OFDM subcarriers are used at once. Such protocols are used in IEEE802.11a and IEEE802.16a, for example. An alternative is to used OFDMA or clustered OFDM, where each connection uses a subset of the OFDM subcarriers. Such an approach is used in some operating modes of IEEE802.16a. MAC protocols generally must support hundreds of end-user terminals that demand a mixture of services ranging from traditional voice and data, internet protocol (IP) connectivity, multimedia and real time applications such as voice-over IP (VoIP). The support of these services requires a MAC protocol that handles both continuous and bursty traffic with quality-of-service (QoS) guarantees that depend on the application. The issues of transport efficiency are addressed at the interface between the MAC and PHY layers, and the actual throughput that is achieved is highly dependent on the choice of MAC protocol. For example, the MAC adjust PHY layer parameters such as the type of modulation and coding employed to meet QoS and link availability requirements. Addition information on typical MAC related issues are available in a variety of sources including the IEEE802.16a standard [2].

X. SOFTWARE RADIO IMPLEMENTATION

The proliferation of high-performance DSP cores, FPGAs, and application-specific integrated circuits (ASICs)—as well as the current trend toward system-on-a-chip (SoC) integration—are bringing the software radio paradigm closer to practical realization. While advances in these key technology areas—and other areas such as wideband A/Ds, low-power circuit technology, and wideband amplifiers—are critical in the evolution of software radio, technology today allows one to begin to discover and appreciate the great promise that software radio holds. Current trends in the wireless telecommunications industry are steering toward advanced applications requiring wider bandwidth, which will place increasing processing loads upon future SDR implementation architectures.

Faculty at Georgia Tech are collaborating to develop a high bandwidth, high data rate wireless gateway using advanced technologies including software radio, smart antennas, MIMO-OFDM, advanced FECs, and higher layers that support quality of service. A key component in the research is the implementation of the techniques in a programmable testbed at the GT Software Radio Laboratory. In this paper, we focus on a description of the physical layer and on the implementation of MIMO-OFDM in the testbed.

In the first part of this section, we describe the design and performance of the software-radio testbed, which was developed using commercial components to implement programmable transceivers for wireless communications. The system provides a useful vantage point for empirical exploration of issues related to software radio implementation. We describe the major hardware components, the algorithm flow through the system, and the implementation performance for MIMO-OFDM.

A. Software Radio Overview

Software radio, as discussed in this section, refers to a transceiver with radio receive and/or transmit functions defined in software. Given the current state of technology, software-defined radio functions are typically employed in the intermediate frequency (IF) and baseband subsystems. Often, software-defined functions are supported with complementary technologies, including programmable devices, such as FPGAs, which can perform certain functions—e.g., down-conversion, FFTs, and FEC decoding—more efficiently than software-defined functions in processing cores. In future "software-defined radio" (SDR), software-defined functions and programmable features would be reconfigurable either through over-the-air commands or via adaptive circuitry allowing a mobile transceiver to seamlessly reconfigure itself based on the electromagnetic environment or other cues available to a transceiver [71].

The programmable functions and features of the testbed are not entirely mature, but do provide a reasonable degree of programming flexibility. As might be expected, the most flexible portions for defining radio functions in our system are those implemented in baseband DSPs. Programming flexibility of the system diminishes as one moves from baseband operations (with DSP and FPGA processing) toward the RF end. In the IF section, the system can employ programmable digital down-converters, DSPs, and leverage FPGAs to implement algorithms. The system is least flexible in the radio frequency (RF) front end of the system, where the RF equipment offers programmable control of tuning frequency and input and output signal attenuations. Following conventional wisdom, the programmable hardware is more easily reconfigured over a limited range of operation but does not offer the same flexibility that software-defined functions afford. The advantage of software-defined functions, however, is balanced by challenges presented by real-time implementation issues: the engineer is faced with the task of defining and then implementing algorithms for real-time operation with constraints imposed by buffering, data input/output (I/O) throughput, bus architectures and capacity, processing speeds, and memory size and access times.

B. Testbed Architecture

The testbed configuration, shown in Fig. 19, consists of two software radio platforms, host PCs for programming and controlling software radio functions, PCs to support MAC and the MAC/IP interface, an Ethernet hub, and PCs hosting client and server applications.

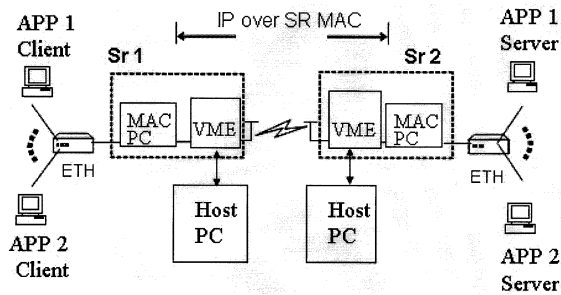The software radio platform architecture is depicted in Fig. 20. The design is based in part on the architecture
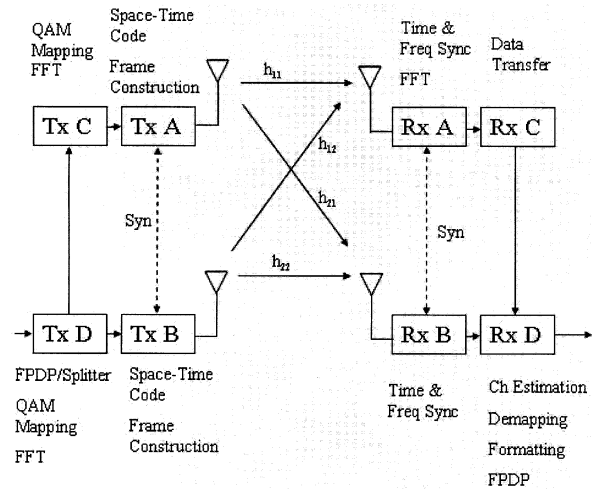
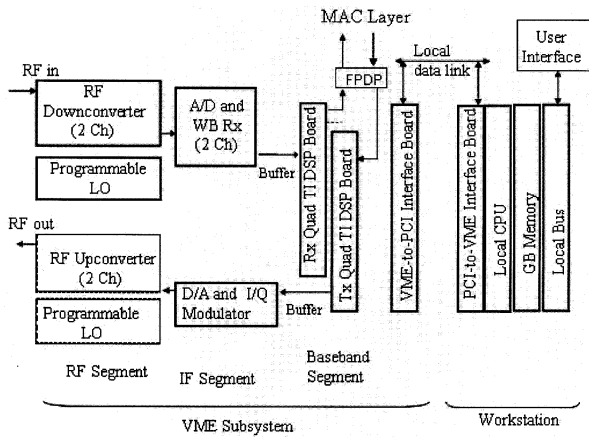**Fig. 19.** Software radio testbed configuration.

Fig. 20. Software radio platform configuration.

proposed by Mitola [72]. The radio physical layers are implemented in a VME rack system populated with commercial off-the-shelf boards to provide functions associated with RF/baseband down- and up-conversion, analog to digital conversion, digital-to-analog converters, and IF and baseband processing.

C. MIMO-OFDM Implementation

Software radio-based implementations of OFDM have been reported in the literature (see, for example, [73]–[78]). But, as yet, software radio implementations for MIMO-OFDM do not appear to be prevalent. In our implementation, the software radios were configured to implement a 2×2 space–time coded MIMO-OFDM system, shown in Fig. 21, based on Alamouti's approach [4]. A more complete description of the system is presented in [79]. The left side of the figure depicts the transmitter on a single Quad DSP board. The input to the board is derived from the MAC layer imbedded in a PC through an FPDP I/O link. The transmit functions include data parallelization, QAM mapping, IFFT transformation, space–time coding, and framing. Algorithms associated with these functions are implemented among processors A,B, C, and D, where the functions are distributed as presented in the figure.

The receive functions include time synchronization, frequency offset estimation and compensation, channel estimation and compensation, and symbol demodulation and QAM demapping. These functions are implemented in a separate quad DSP board, where the algorithms are distributed among
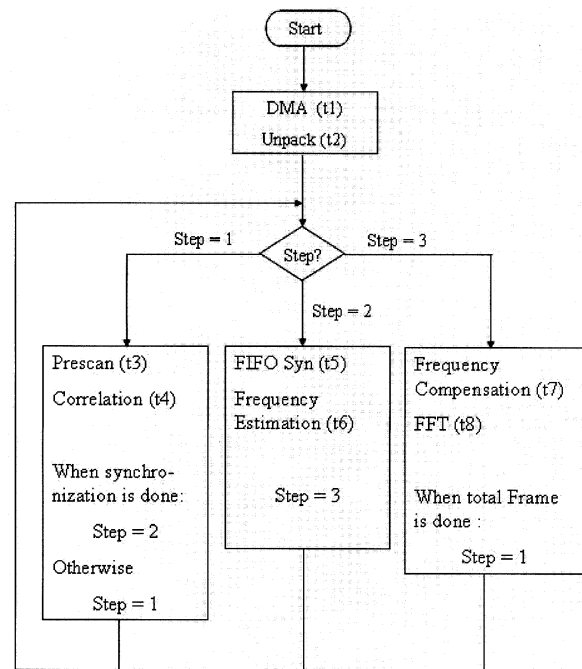

Fig. 21. The configuration of 2×2 MIMO-OFDM space–time system.

Fig. 22. The data flow chart of Rx_A.

processors A, B, C, and D according to the figure. The output of this board is passed through an FPDP I/O link to the receive MAC processor that resides in a PC.

Typically, receiver processing requires greater computational horsepower than transmit processing, due in large part to synchronization and FEC decoding (if present). The data flow associated with the MIMO-OFDM receive functions in the DSPs are illustrated in Figs. 22 and 23. Fig. 22 shows the processing functions/algorithms associated with Processor A. The same processing is employed in Processor B. Fig. 23 shows the processing associated with Processor D. Processor C serves as a buffer for delivering the output data from Processor A into Processor D.

The associated time budgets associated with the functions are listed in Table 2, where the alphanumeric designation
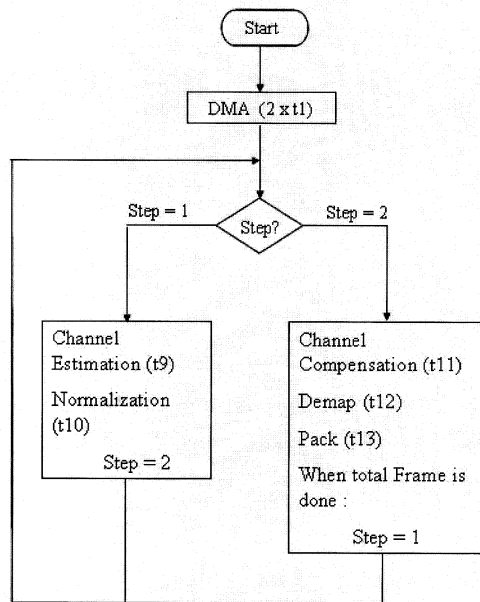
Fig. 23. The data flow chart of Rx_D.

Table 2
Function Time Budgets

	Processing	Time Budget in Cycles 1Cycle = 1/167MHz = 5.988ns
t1	DMA Transfer of 320 Complex Samples Complex Samples from IO FIFO to IDRAM	320C
t2	Unpacking 320 Complex Samples to IQ (in idram)	1KC
t3	Detect the approximate frame start sample using energy	2KC
t4	Use cross-correlation to find the frame start sample	3KC
t5	FIFO synchronization to OFDM symbols	¡640C
t6	Frequency estimation	3KC
t7	Frequency Compensation	3KC
t8	FFT (radix 4) and bit reversal	4KC + 800C
t9	Channel Estimation	9KC
t10	Normalization	3KC
t11	Channel Compensation	3KC
t12	64 QAM De-mapping	3KC
t13	Packing	3KC
Ta	Complex Conjugate Vector Production (256 Complex Numbers)	700C
Tb	Complex Vector Production (256 Complex Numbers)	700C
Tc	Vector Sum (256 Complex Numbers)	700C

"$t\#$" in the table corresponds to the processing function indicated in the figures above. The time budgets for each function are presented in terms of clock cycles, where each cycle corresponds roughly to 6 ns.

Following synchronization, the maximum achievable throughput of the system depends upon the maximum processing time required by any one processor in the pipeline to process an OFDM symbol. Based on the chart above, one of the processors requires roughly 5 KC for FFT computations, indicating that the system can support complex sample rates as high as 10 MHz.

D. System Expansion

System scalability was a key design consideration in the development of the testbed system. The MIMO-OFDM system is now undergoing modification to incorporate new features to increase the system bandwidth and the spectral efficiency of the system, and to improve the interference performance and reliability of the system. Power-PC-based processing boards are being integrated into the system to replace the DSP-based processing boards. The new boards offer processing efficiency increases for many functions, particularly for algorithms that can be vectorized. Example gains that have been demonstrated in the system include FFT speeds that are nearly four times faster than with the DSP boards. Spectral efficiency is to be increased through the utilization of BLAST-type algorithms in a 4×4 MIMO-OFDM system. Interference suppression will be achieved with beamswitching antennas that monitor the SINR on each channel. FEC is also being integrated in FPGAs, where proprietary FEC cores for Reed–Solomon coding are initially being deployed, but where more advanced FEC cores are planned for integration in the future.

E. Extensions to System on a Chip

We have described the implementation and processing performance of a MIMO-OFDM system in a software radio testbed. The specific architecture of the system, including the bus design, processor interconnectivity, board interconnectivity, the memory resources, access times, and arbitration, and the processing resources associated with the system are largely inflexible and depend on specific vendor designs. Parallel work to the testbed integration work is also being conducted to evaluate alternative bus architectures, memory arbitration, and custom logic in heterogenous multiprocessor environments [80], [81]. The purpose of these studies is to determine architectures to enhance the system performance for SoC multiprocessor implementations. This work is particularly relevant to the design of future SDR systems, which may eventually demand implementation architectures that are scalable (e.g., to accommodate increased transmission bandwidths), and flexible (e.g., to accommodate new functions and algorithms).

XI. Conclusion

This paper has discussed a number of PHY layer issues relevant for the implementation of broadband MIMO-OFDM systems. We have discussed in detail the peculiar issues relating to MIMO-OFDM synchronization and channel estimation. We then discussed space–time coding strategies for closed loop MIMO-OFDM systems where knowledge of the channel is available at the transmitter. Error correction coding was discussed with an emphasis on high-rate LDPC codes. Adaptive analog beam forming techniques were discussed that can provide the best possible MIMO channel environment. Finally, the paper discussed a software radio test bed at Georgia Tech for MIMO-OFDM.

REFERENCES

[1] *Part 11: Wireless LAN Medium Access Control (MAC) and Physical Layer (PHY) Specifications: High-Speed Physical Layer in the 5 GHz Band*, IEEE Standard 802.11a-1999.

[2] *Local and Metropolitan Area Networks—Part 16, Air Interface for Fixed Broadband Wireless Access Systems*, IEEE Standard IEEE 802.16a.

[3] L. J. Cimini, Jr., "Analysis and simulation of a digital mobile channel using orthogonal frequency division multiplexing," *IEEE Trans. Commun.*, vol. COM-33, pp. 665–675, July 1985.

[4] S. Alamouti, "A simple transmit diversity technique for wireless comminications," *IEEE J. Select. Areas Commun.*, vol. 16, pp. 1451–1458, Oct. 1998.

[5] V. Tarokh, H. Jafarkhani, and A. R. Calderbank, "Space–time block codes from orthogonal designs," *IEEE Trans. Inform. Theory*, vol. 45, pp. 1456–1467, July 1999.

[6] V. Tarokh, N. Seshadri, and A. R. Calderbank, "Space–time codes for high data rate wireless communication: Performance criterion and code construction," *IEEE Trans. Inform. Theory*, vol. 44, pp. 744–765, Mar. 1998.

[7] P. W. Wolniansky, G. J. Foschini, G. D. Golden, and R. A. Valenzuela, "V-Blast: An architecture for realizing very high data rates over the rich-scattering channel," in *Proc. Int. Symp. Signals, Systems and Electronics (ISSE 1998)*, pp. 295–300.

[8] J. Ha, A. N. Mody, J. H. Sung, J. Barry, S. Mclaughlin, and G. L. Stuber, "LDPC coded OFDM with Alamouti/SVD diversity technique," *J. Wireless Pers. Commun.*, vol. 23, no. 1, pp. 183–194, Oct. 2002.

[9] G. G. Raleigh and J. M. Cioffi, "Spatio-temporal coding for wireless communcation," *IEEE Trans. Commun.*, vol. 46, pp. 357–366, Mar. 1998.

[10] D. Agrawal, V. Tarokh, A. Naguib, and N. Seshadri, "Space–time coded OFDM high data-rate wireless communication over wideband channels," in *Proc. IEEE Vehicular Technology Conf.*, 1998, pp. 2232–2236.

[11] H. Bölcskei and A. Paulraj, "Space-frequency coded broadband OFDM systems," in *Proc. IEEE Wireless Communications Networking Conf.*, 2000, pp. 1–6.

[12] B. Lu and X. Wang, "Space–time code design in OFDM systems," in *Proc. Globecom*, vol. 2, 2000, pp. 1000–1004.

[13] H. Bölcskei and A. Paulraj, "Space-frequency codes for broadband fading channels," in *Proc. IEEE Int. Symp. Info. Theory*, 2001, p. 219.

[14] H. Bölcskei, M. Borgmann, and A. Paulraj, "Space-frequency coded MIMO-OFDM with variable multiplexing-diversity tradeoff," presented at the IEEE Int. Conf. Communications (ICC), Anchorage, AK, 2003.

[15] Y. Liu, M. P. Fitz, and O. Y. Takeshita, "Space time codes: Performance criteria and design for frequency selective fading channels," in *Proc. IEEE Int. Conf. Communications (ICC)*, vol. 9, 2001, pp. 2800–2804.

[16] H. El Gamal, A. R. Hammons, Jr., Y. Liu, M. P. Fitz, and O. Y. Takeshita, "On the design of space–time and space-frequency codes for MIMO frequency selective fading channels," IEEE Trans. Inform. Theory, vol. 49, pp. 2277–2292, Sept. 2003.

[17] Z. Liu, Y. Xin, and G. Giannakis, "Space–time-frequency coded OFDM over frequency-selective fading channels," *IEEE Trans. Signal Processing*, vol. 50, pp. 2465–2476, Oct. 2002.

[18] M. Guillaud and D. Slock, "Full-rate full-diversity space-frequency coding for MIMO OFDM systems," in *Proc. IEEE Benelux Signal Processing Symp.*, 2002, pp. S02–14.

[19] Y. (G.) Li, J. H. Winters, and N. R. Sollenberger, "MIMO-OFDM for wireless communications: Signal detection with enhanced channel estimation," *IEEE Trans. Commun.*, vol. 50, pp. 1471–1477, Sept. 2002.

[20] S. Kaiser, "Spatial transmit diversity techniques for broadband OFDM systems," in *Proc. IEEE Globecom*, 2000, pp. 1824–1828.

[21] A. Dammann and S. Kaiser, "Standard conformable antenna diversity techniques for OFDM and its application to the DVB-T system," in *Proc. IEEE Globecom*, 2001, pp. 3100–3105.

[22] A. Dammann, P. Lusina, and M. Bossert, "On the equivalence of space–time block coding with multipath propagation and/or cyclic delay diversity in OFDM," in *Proc. Eur. Wireless 2002*, pp. 847–851.

[23] J. Tan and G. L. Stüber, "Multicarrier delay diversity modulation for MIMO systems," *IEEE Trans. Wireless Commun.*, to be published.

[24] A. N. Mody and G. L. Stuber, "Efficient training and synchronization sequence structures for MIMO OFDM systems," presented at the 6th OFDM Workshop 2001, Hamburg, Germany.

[25] ——, "Synchronization for MIMO OFDM systems," in *Proc. Globecom 2001*, pp. 509–513.

[26] V. Tarokh, H. Jafarkhani, and A. R. Calderbank, "Space–time block coding for wireless communications: Performance results," *IEEE J. Select. Areas Commun.*, vol. 17, pp. 451–460, Mar. 1999.

[27] A. N. Mody and G. L. Stuber, "Sampling frequency offset estimation and time tracking for MIMO OFDM systems," presented at the 8th OFDM Workshop 2003, Hamburg, Germany.

[28] ——, "Receiver implementation for a MIMO OFDM system," in *Proc. Global Communications Conference (Globecom 2002)*, vol. 1, pp. 716–720.

[29] T. M. Schmidl and D. C. Cox, "Robust frequency and timing synchronization for OFDM," *IEEE Trans. Commun.*, vol. 45, pp. 1613–1621, Dec. 1997.

[30] B. Yang, K. B. Letaief, R. S. Cheng, and Z. Cao, "Timing recovery for OFDM transmission," *IEEE J. Select. Areas Commun.*, vol. 18, pp. 2278–2291, Nov. 2000.

[31] Y. (G.) Li, N. Seshadri, and S. Ariyavisitakul, "Channel estimation for OFDM systems with transmitter diversity in mobile wireless channels," *IEEE J. Select. Areas Commun.*, vol. 17, pp. 461–471, Mar. 1999.

[32] Y. (G.) Li, L. J. Cimini, Jr., and N. R. Sollenberger, "Robust channel estimation for OFDM systems with rapid dispersive fading channels," *IEEE Trans. Commun.*, vol. 46, pp. 902–915, July 1998.

[33] Y. (G.) Li, "Simplified channel estimation for OFDM systems with multiple transmit antennas," *IEEE Trans. Wireless Commun.*, vol. 1, pp. 67–75, Jan. 2002.

[34] A. Wittneben, "A new bandwidth efficient transmit antenna modulation diversity scheme for linear digital modulation," in *Proc. IEEE Int. Conf. Communications*, 1993, pp. 1630–1634.

[35] N. Seshadri and J. H. Winters, "Two signaling schemes for improving the error performance of frequency-division-duplex (FDD) transmission systems using transmitter antenna diversity," *Int. J. Wireless Inform. Networks*, vol. 1, pp. 24–47, Jan. 1994.

[36] J. H. Winters, "The diversity gain of transmit diversity in wireless systems with Rayleigh fading," in *Proc. IEEE Int. Conf. Communications*, 1994, pp. 1121–1125.

[37] ——, "The diversity gain of transmit diversity in wireless systems with Rayleigh fading," *IEEE Trans. Veh. Technol.*, vol. 47, pp. 119–123, Feb. 1998.

[38] X. Zhu and R. D. Murch, "Performance analysis of maximum likelihood detection in a MIMO antenna system," *IEEE Trans. Commun.*, vol. 50, pp. 187–191, Feb. 2002.

[39] A. Duel-Hallen, "Equalizers for multiple input/multiple output channels and PAM systems with cyclostationary input sequences," *IEEE J. Select. Areas Commun.*, vol. 10, pp. 630–639, Apr. 1992.

[40] J. H. Sung and J. R. Barry, "Bit-allocation strategies for MIMO fading channels with channel knowledge at the transmitter," presented at the Spring VTC, Jeju, Korea, 2003.

[41] ——, "Bit-allocation strategies for closed-loop MIMO OFDM," presented at the Vehicular Technology Conf. (VTC'03), Orlando, FL.

[42] R. G. Gallager, *Low-Density Parity-Check Codes*. Cambridge, MA: MIT Press, 1963.

[43] D. J. C. MacKay, "Good error-correcting codes based on sparse very matrices," *IEEE Trans. Inform. Theory*, vol. 45, pp. 399–431, Mar. 1999.

[44] J. Ha, J. Kim, and S. W. McLaughlin, "Rate compatible puncturing of LDPCs," *IEEE Trans. Inform. Theory*, to be published.

[45] C. Jones, T. Tian, A. Matache, R. Wesel, and J. Villasenor, "Robustness of LDPCs on periodic fading channels," presented at the Globecom 2002, Taipei, Taiwan, R.O.C.

[46] L. Goulet and H. Leib, "Serially concatenated spacetime codes with iterative decoding and performance limits of block-fading channels," *IEEE J. Select. Areas Commun.*, vol. 21, pp. 765–773, June 2003.

[47] A. Stefanov and T. Duman, "Performance bounds for turbo-coded multiple antenna systems," *IEEE J. Select. Areas Commun.*, vol. 21, pp. 374–381, Apr. 2003.

[48] B. Hassibi and B. Hochwald, "High-rate codes that are linear in space and time," *IEEE Trans. Inform. Theory*, vol. 48, pp. 1804–1825, July 2002.

[49] W. Su, Z. Safar, M. Olfat, and R. Liu, "Obtaining full-diversity space-frequency codes from space–time codes via mapping," *IEEE Trans. Signal Processing*, vol. 51, pp. 2905–2916, Nov. 2003.

[50] K. Lee and D. Williams, "A space-frequency transmitter diversity technique for OFDM systems," in *Proc. Globecom*, vol. 3, 2000, pp. 1473–1477.

[51] R. Blum, Y. (G.) Li, J. Winters, and Q. Yam, "Improved space–time coding for MIMO-OFDM wireless communications," *IEEE Trans. Commun.*, vol. 49, pp. 1873–1878, Nov. 2001.

[52] Y. Gong and K. Letaief, "An efficient space-frequency coded wideband OFDM system for wireless communications," in *Proc. ICC*, vol. 1, 2002, pp. 475–479.

[53] B. Lu, X. Wang, and K. Narayanan, "LDPC-based space–time coded OFDM systems over correlated fading channels: Performance analysis and receiver design," *IEEE Trans. Commun.*, vol. 50, pp. 74–88, Jan. 2002.

[54] Y. Liu and M. Fitz, "Space–time turbo codes," presented at the 37th Annu. Allerton Conf., Monticello, IL, 1999.

[55] R. W. Heath, S. Sandhu, and A. Paulraj, "Antenna selection for spatial multiplexing systems with linear receivers," *IEEE Commun. Lett.*, vol. 5, pp. 142–144, Apr. 2001.

[56] D. Gore and A. Paulraj, "Space–time block coding with optimal antenna selection," in *Proc. IEEE Int. Conf. Acoustics, Speech, and Signal Processing*, vol. 4, 2001, pp. 2441–2444.

[57] R. S. Blum and J. H. Winters, "On optimum MIMO with antenna selection," in *Proc. IEEE Int. Conf. Communications*, vol. 1, 2002, pp. 386–390.

[58] ——, "On optimum MIMO with antenna selection," *IEEE Commun. Lett.*, vol. 6, pp. 322–324, Aug. 2002.

[59] K. U-yen, J. S. Kenney, and T. Assavapokee, "An optimization technique for low-loss nXm microwave switch matrices," presented at the 2003 IEEE Radio and Wireless Conf. (RAWCON), Boston, MA.

[60] H. Shi, M. Katayama, T. Yamazato, H. Okada, and A. Ogawa, "An adaptive antenna selection scheme for transmit diversity in OFDM systems," in *Proc. IEEE Vehicular Technology Conf.*, vol. 4, 2001, pp. 2168–2172.

[61] H. Asplund, A. F. Molisch, M. Steinbauer, and N. B. Mehta, "Clustering of scatterers in mobile radio channels—Evaluation and modeling in the COST259 directional channel model," in *Proc. IEEE Int. Conf. Communications*, vol. 2, 2002, pp. 901–905.

[62] C.-C. Chong, C.-M. Tan, D. I. Laurenson, S. McLaughlin, M. A. Beach, and A. R. Nix, "A new statistical wideband spatio-temporal channel model for 5-GHz band WLAN systems," *IEEE J. Select. Areas Commun*, vol. 21, pp. 139–150, Feb. 2003.

[63] J. H. Winters and M. J. Gans, "The range increase of adaptive versus phased arrays in mobile radio systems," *IEEE Trans. Veh. Technol.*, vol. 48, pp. 353–362, Mar. 1999.

[64] R. J. Mailloux, *Phase Array Antenna Handbook*. New York: Artech House Inc., 1994.

[65] F. Caldwell, J. S. Kenney, and M. A. Ingram, "Design and implementation of a switched-beam smart antenna for an 802.11b wireless access point," presented at the 2002 IEEE Radio and Wireless Conf. (RAWCON), Boston, MA.

[66] K.-H. Li, M. A. Ingram, and E. O. Rausch, "Multibeam antennas for indoor wireless communications," *IEEE Trans. Commun.*, vol. 50, pp. 192–194, Feb. 2002.

[67] K.-H. Li and M. A. Ingram, "Space–time block-coded OFDM systems with RF beamformers for high-speed indoor wireless communications," *IEEE Trans. Commun.*, vol. 50, pp. 1899–1901, Dec. 2002.

[68] L. Dong and M. A. Ingram, "Beam selection algorithm based on PTR metric and its synchronization performance," presented at the 2003 IEEE Radio and Wireless Conf. (RAWCON), Boston, MA.

[69] J.-S. Jiang and M. A. Ingram, "Comparison of beam selection and antenna selection techniques in indoor MIMO systems at 5.8 GHz," presented at the 2003 IEEE Radio and Wireless Conf. (RAWCON), Boston, MA.

[70] M. F. Demirkol and M. A. Ingram, "Stream control in networks with interfering MIMO links," presented at the IEEE Wireless Communications and Networking Conf. (WCNC), New Orleans, LA, 2003.

[71] Software defined radio forum [Online]. Available: http://www.sdr-forum.org

[72] J. Mitola, "The software radio architecture," *IEEE Commun. Mag.*, vol. 33, pp. 26–38, May 1995.

[73] E. Sereni *et al.*. A software radio OFDM transceiver for WLAN applications. [Online]. Available: http://www.di.uoa.gr/speech/dsp/X/PERUGI.PDF

[74] S. Gifford, J. Kleider, and S. Chuprin, "Broadband OFDM using 16-bit precision on a SDR platform," in *Proc. MILCOM 2001*, pp. 180–184.

[75] K.-C. Chen and S.-T. Wu, "A programmable architecture for OFDM-CDMA," *IEEE Commun. Mag.*, vol. 37, no. 11, pp. 76–82, Nov. 1999.

[76] J. D. Bakker and F. C. Schoute, "LART: Design and implementation of an experimental wireless platform," in *Proc. IEEE VTC 2000*, pp. 1460–1466.

[77] M. F. Tariq *et al.*, "Development of an OFDM based hgh-speed wireless LAN platform using the TI C6X DSP," in *Proc. IEEE Int. Conf. Communications*, 2002, pp. 522–526.

[78] K. Witrisal *et al.*, "Air-interface emulation for wireless broadband communications applied to OFDM," in *Proc. Personal, Indoor and Mobile Radio Communications*, 2000, pp. 1251–1255.

[79] W. Xiang, T. Pratt, N. Jones, X. Wang, L. Dong, and T. l. Zhang, "A software radio MIMO-OFDM prototype for broadband wireless access, part I: System architecture", submitted for publication.

[80] K. K. Ryu, E. Shin, and V. J. Mooney, III, "A comparison of five different multiprocessor SoC bus architectures," in *Proc. Euromicro Symp. Digital Systems Design*, 2001, pp. 202–209.

[81] B. E. Saglam and V. J. Mooney, III, "System-on-a-chip processor synchronization support in hardware," in *Proc. Design, Automation and Test in Europe*, 2001, pp. 633–639.

Gordon L. Stüber (Fellow, IEEE) received the B.A.Sc. and Ph.D. degrees in electrical engineering from the University of Waterloo, Waterloo, ON, Canada, in 1982 and 1986 respectively.

Since 1986, he has been with the School of Electrical and Computer Engineering, Georgia Institute of Technology, Atlanta, where he is currently the Joseph M. Pettit Professor in Communications. He is the author of *Principles of Mobile Communication,* (Norwell, MA: Kluwer, 1996, 2nd ed. 2001). His research interests are in wireless communications and communication signal processing.

Dr. Stüber was Corecipient of the Jack Neubauer Memorial Award in 1997 recognizing the best systems paper published in the IEEE TRANSACTIONS ON VEHICULAR TECHNOLOGY. He received the IEEE Vehicular Technology Society James R. Evans Avant Garde Award in 2003 recognizing his contributions to theoretical research in wireless communications. He served as Technical Program Chair for the 1996 IEEE Vehicular Technology Conference (VTC'96), Technical Program Chair for the 1998 IEEE International Conference on Communications (ICC'98), General Chair of the Fifth IEEE Workshop on Multimedia, Multiaccess and Teletraffic for Wireless Communications (MMT2000), General Chair of the 2002 IEEE Communication Theory Workshop, and and General Chair of the Fifth International Symposium on Wireless Personal Multimedia Communications (WPMC2002). He is a past Editor for Spread Spectrum with the IEEE TRANSACTIONS ON COMMUNICATIONS (1993–1998), and a past member of the IEEE Communications Society Awards Committee (1999–2002). He is currently an elected member of the IEEE Vehicular Technology Society Board of Governors (2001–2003, 2004–2006).

John R. Barry (Member, IEEE) received the B.S. degree in electrical engineering from the State University of New York, Buffalo, in 1986 and the M.S. and Ph.D. degrees in electrical engineering from the University of California, Berkeley, in 1987 and 1992, respectively.

Since 1992, he has been with the Georgia Institute of Technology, Atlanta, where he is an Associate Professor with the School of Electrical and Computer Engineering. His research interests include wireless communications, equalization, and multiuser communications. He is a coauthor with E. A. Lee and D. G. Messerschmitt of *Digital Communications, Third Edition*, (Norwell, MA: Kluwer, 2004), and the author of *Wireless Infrared Communications* (Norwell, MA: Kluwer, 1994).

Steve W. McLaughlin (Senior Member, IEEE) received the B.S. degree from Northwestern University, Evanston, IL, in 1985, the M.S.E. degree from Princeton University, Princeton, NJ, in 1986, and the Ph.D. degree from the University of Michigan, Ann Arbor, in 1992.

From 1992 to 1996, he was on the electrical engineering faculty at the Rochester Institute of Technology, Rochester, NY. Since 1996, he has been with the School of Electrical and Computer Engineering, Georgia Institute of Technology, Atlanta. He is also a Principal Scientist at Calimetrics, Inc. He coedited (with S. Verdu) *Information Theory: 50 Years of Discovery* (New York: IEEE Press, 1999). His research interests are in the area of communications and information theory. Specific interests are in turbo and constrained codes for magnetic and optical recording, FEC and equalization for optical networks, theory of error control coding, and source coding (quantization and compression).

Dr. McLaughlin received the Presidential Early Career Award for Scientists and Engineers (PECASE) where he was cited by U.S. President Bill Clinton "for leadership in the development of high-capacity, nonbinary optical recording formats." He also received the National Science Foundation CAREER award for this work. He is currently Second Vice President of the IEEE Information Theory Society. From 1995 to 1999, he served as the Publications Editor for the IEEE TRANSACTIONS ON INFORMATION THEORY. He has also served on the IEEE Publications Activities Board (1998–2001) and is a former Secretary of the IEEE Atlanta Section (2000).

Mary Ann Ingram (Senior Member, IEEE) received the B.E.E. and Ph.D. degrees from the Georgia Institute of Technology, Atlanta, in 1983 and 1989, respectively.

From 1983 to 1986, she was a Research Engineer with the Georgia Tech Research Institute, performing studies on radar electronic countermeasure (ECM) systems. In 1986, she became a Graduate Research Assistant with the School of Electrical and Computer Engineering at Georgia Tech, where in 1989, she became a Faculty Member and is currently an Associate Professor. Her early research areas were optical communications and radar systems. Since 1997, her research interest has been the application of multiple antenna systems to wireless communications. In particular, she and her students have investigated the use of RF beamformers and RF switches in MIMO and adaptive array architectures, wideband MIMO channel measurement and stochastic modeling, multiantenna architectures for semipassive RF tags and their interrogators, and cross-layer algorithm development for networks with interfering MIMO links. Many of these projects involve the design and construction of hardware prototypes.

Ye (Geoffrey) Li (Senior Member, IEEE) received the B.S.E. and M.S.E. degrees in 1983 and 1986, respectively, from the Department of Wireless Engineering, Nanjing Institute of Technology, Nanjing, China, and the Ph.D. degree in 1994 from the Department of Electrical Engineering, Auburn University, Auburn, AL.

He was with AT&T Labs—Research. Since 2000, he has been an Associate Professor at Georgia Institute of Technology, Atlanta. His general research interests include statistical signal processing and wireless communications. In these areas, he has contributed over 100 papers published in referred journals and presented in various international conferences. He also has over 10 U.S. patents granted or pending.

Dr. Li was a Guest Editor for two special issues on Signal Processing for Wireless Communications for the IEEE JOURNAL ON SELECTED AREAS IN COMMUNICATIONS. He is currently serving as an Editor for Wireless Communication Theory for the IEEE TRANSACTIONS ON COMMUNICATIONS. He organized and chaired many international conferences, including Technical Program Vice-Chair of IEEE 2003 International Conference on Communications.

Thomas Pratt (Member, IEEE) received the B.S. degree from the University of Notre Dame, Notre Dame, IN, in 1985 and the M.S. and Ph.D. degrees in electrical engineering from the Georgia Institute of Technology, Atlanta, in 1989 and 1999, respectively.

He is Head of the software radio laboratory at Georgia Tech, where research has focused principally on MIMO-OFDM, space–time adaptive processing, WLAN coexistence and interference suppression, GSM receivers, and channel modeling for mobile communications. He is a Senior Research Engineer at the Georgia Tech Research Institute.